

Dear Editor:

We would like to thank the editor and two anonymous reviewers for their constructive comments, which significantly improved this manuscript. Below, we address all comments point-by-point in **blue**.

Anonymous Referee #2.

General:

The paper has improved significantly as compared to the first version. Nevertheless, there are still some issues where the paper needs further improvement before it can finally be published. Although the majority of the reviewer comments are sufficiently addressed there are still some aspects which must be highlighted in more detail. Another deficiency of the paper is still the language quality of some (but not all) parts of the paper. Here, the authors with better knowledge of the English language as well as the native speaker are requested put some effort into improving those sections which are still not well written or a language editing service should be consulted.

Response: We (including native speaker) have read the manuscript very carefully and edited the language. Hope the language quality has been improved.

Detailed comments:

Line 43: Differences among the simulated chemical composition of the aerosol are not solely due to different description of the chemistry.

Response: We removed “, which is due to different parameterizations of chemical reactions” and added “However, it was also found that the ensemble mean of the models produced the best prediction skill in most cases. While this has been shown for other conditions (for example prediction of high ozone events in the US, this is to our knowledge the first time it has been shown for heavy haze events” in the abstract.

Page 9 - 11: References are not complete please check (not only for these pages but everywhere). For example, references are missing for RADM2, RACM, MADE/SORGAM, AE6.

Response: We add the references for RACM (Stockwell et al., 1997), RADM2 (Stockwell et al., 1990), MADE/SORGAM (Ackermann et al., 1998, Schell et al., 2001), AE6 (Carlton et al., 2010).

Ackermann, I.J., Hass, H., Memmesheimer, M., Ebel, A., Binkowski, F.S. and Shankar, U.M.A., 1998. Modal aerosol dynamics model for Europe: Development and first applications. *Atmospheric environment*, 32(17), pp.2981-2999.

Schell, B., Ackermann, I.J., Hass, H., Binkowski, F.S. and Ebel, A., 2001. Modeling the formation of secondary organic aerosol within a comprehensive air quality model system. *Journal of Geophysical Research: Atmospheres*, 106(D22), pp.28275-28293

Stockwell, W.R., Middleton, P., Chang, J.S. and Tang, X., 1990. The second generation regional acid deposition model chemical mechanism for regional air quality

modeling. *Journal of Geophysical Research: Atmospheres*, 95(D10), pp.16343-16367.

Stockwell, W. R., et al. (1997). "A new mechanism for regional atmospheric chemistry modeling." *Journal of Geophysical Research: Atmospheres* 102(D22): 25847-25879.

Carlton, A.G., Bhawe, P.V., Napelenok, S.L., Edney, E.O., Sarwar, G., Pinder, R.W., Pouliot, G.A. and Houyoux, M., 2010. Model representation of secondary organic aerosol in CMAQv4. 7. *Environmental science & technology*, 44(22), pp.8553-8560.

For other references, we add Zhao et al., 2016 and Li et al., 2014.

Li, M., Zhang, Q., Streets, D.G., He, K.B., Cheng, Y.F., Emmons, L.K., Huo, H., Kang, S.C., Lu, Z., Shao, M. and Su, H., 2014. Mapping Asian anthropogenic emissions of non-methane volatile organic compounds to multiple chemical mechanisms. *Atmospheric Chemistry and Physics*, 14(11), p.5617.

Zhao, B., Wang, S., Donahue, N.M., Jathar, S.H., Huang, X., Wu, W., Hao, J. and Robinson, A.L., 2016. Quantifying the effect of organic aerosol aging and intermediate-volatility emissions on regional-scale aerosol pollution in China. *Scientific reports*, 6, p.28815.

Ginoux, P., Chin, M., Tegen, I., Prospero, J.M., Holben, B., Dubovik, O. and Lin, S.J., 2001. Sources and distributions of dust aerosols simulated with the GOCART model. *Journal of Geophysical Research: Atmospheres*, 106(D17), pp.20255-20273.

Kalnay, E., Kanamitsu, M., Kistler, R., Collins, W., Deaven, D., Gandin, L., Iredell, M., Saha, S., White, G., Woollen, J. and Zhu, Y., 1996. The NCEP/NCAR 40-year reanalysis project. *Bulletin of the American meteorological Society*, 77(3), pp.437-471.

Randerson, J.T., G.R. van der Werf, L. Giglio, G.J. Collatz, and P.S. Kasibhatla. 2015. Global Fire Emissions Database, Version 4 (GFEDv4). ORNL DAAC, Oak Ridge, Tennessee, USA. <http://dx.doi.org/10.3334/ORNLDAAAC/1293>

Lin, Y.L., Farley, R.D. and Orville, H.D., 1983. Bulk parameterization of the snow field in a cloud model. *Journal of Climate and Applied Meteorology*, 22(6), pp.1065-1092.

Morrison, H., Curry, J.A. and Khvorostyanov, V.I., 2005. A new double-moment microphysics parameterization for application in cloud and climate models. Part I: Description. *Journal of the Atmospheric Sciences*, 62(6), pp.1665-1677.

Tao, W.K., Simpson, J., Baker, D., Braun, S., Chou, M.D., Ferrier, B., Johnson, D., Khain, A., Lang, S., Lynn, B. and Shie, C.L., 2003. Microphysics, radiation and surface processes in the Goddard Cumulus Ensemble (GCE) model. *Meteorology and Atmospheric Physics*, 82(1), pp.97-137.

Reisner, J., RaSmuSSen, R.M. and Brientjes, R.T., 1998. Explicit forecasting of supercooled liquid water in winter storms using the MM5 mesoscale model. *Quarterly*

Journal of the Royal Meteorological Society, 124(548), pp.1071-1107.

Iacono, M.J., Delamere, J.S., Mlawer, E.J., Shephard, M.W., Clough, S.A. and Collins, W.D., 2008. Radiative forcing by long-lived greenhouse gases: Calculations with the AER radiative transfer models. *Journal of Geophysical Research: Atmospheres*, 113(D13).

Mlawer, E.J., Taubman, S.J., Brown, P.D., Iacono, M.J. and Clough, S.A., 1997. Radiative transfer for inhomogeneous atmospheres: RRTM, a validated correlated - k model for the longwave. *Journal of Geophysical Research: Atmospheres*, 102(D14), pp.16663-16682.

Chou, M.D. and Suarez, M.J., 1994. An efficient thermal infrared radiation parameterization for use in general circulation models (p. 85). National Aeronautics and Space Administration, Goddard Space Flight Center.

Maloney, E.D. and Hartmann, D.L., 2001. The sensitivity of intraseasonal variability in the NCAR CCM3 to changes in convective parameterization. *Journal of Climate*, 14(9), pp.2015-2034.

Hong, S.Y. and Pan, H.L., 1996. Nonlocal boundary layer vertical diffusion in a medium-range forecast model. *Monthly weather review*, 124(10), pp.2322-2339.

Grell, G.A., 1993. Prognostic evaluation of assumptions used by cumulus parameterizations. *Monthly Weather Review*, 121(3), pp.764-787.

Ek, M.B., Mitchell, K.E., Lin, Y., Rogers, E., Grunmann, P., Koren, V., Gayno, G. and Tarpley, J.D., 2003. Implementation of Noah land surface model advances in the National Centers for Environmental Prediction operational mesoscale Eta model. *Journal of Geophysical Research: Atmospheres*, 108(D22).

Henderson-Sellers, A., 1993. A factorial assessment of the sensitivity of the BATS land-surface parameterization scheme. *Journal of climate*, 6(2), pp.227-247.

Line 201: This sentence sounds like this was done recently, which is not the case.

Response: We change the sentence to “coupled by Schell et al (2001) was used in M1”

Schell, B., Ackermann, I.J., Hass, H., Binkowski, F.S. and Ebel, A., 2001. Modeling the formation of secondary organic aerosol within a comprehensive air quality model system. *Journal of Geophysical Research: Atmospheres*, 106(D22), pp.28275-28293.

Line 257 – 258: And what about RADM2 and RACM-ESRL?

Response: We add one sentence in the manuscript to describe this: “Speciation mapping of NMVOC emissions for groups using other gas-phase chemical

mechanisms, such as CBMZ, RADM2 and CBM4, used the speciation framework documented in Li et al. (2014).”

Li, M., Zhang, Q., Streets, D.G., He, K.B., Cheng, Y.F., Emmons, L.K., Huo, H., Kang, S.C., Lu, Z., Shao, M. and Su, H., 2014. Mapping Asian anthropogenic emissions of non-methane volatile organic compounds to multiple chemical mechanisms. *Atmospheric Chemistry and Physics*, 14(11), p.5617.

Section 2.2: As some of the models account for dust, a short paragraph on dust emissions should be added as well.

Response: We add the following subsection to describe dust emissions.

2.2.6 Dust emissions

In M2, the Air Force Weather Agency (AFWA) version of the GOCART dust model was used. It calculates the saltation flux as a function of friction velocity (u_*) and threshold friction velocity (u_{*t}):

$$Q = C \frac{\rho_0}{g} u_*^3 \left(1 + \frac{u_{*t}}{u_*}\right) \left(1 - \frac{u_{*t}^2}{u_*^2}\right) \text{ when } u_* \geq u_{*t}$$

where C is a tunable empirical constant, ρ_0 is air density, and g is gravitational acceleration. The bulk vertical dust flux is estimated by $F = \alpha QE$ (Marticorena and Bergametti, 1995), in which α is the sandblasting efficiency and E is the dust erodibility factor. The erodibility factor data is included in the model geography dataset. In M3 and M4, the dust emissions are estimated using the GOCART dust model (Ginoux et al., 2001), which was determined by soil texture, moisture and surface wind speed. The drier the soil and the stronger the wind, the higher dust emissions over the regions where the erodibility factor is not zero. In M5, soil dust emissions were estimated by the approach from Han et al. (2004):

$$F = C_0 u_*^4 \left(1 - \frac{u_{*t}}{u_*}\right) (1 - f_i R_i) \text{ when } u_* \geq u_{*t}, \text{ RH} \leq \text{RHt}$$

C_0 is a constant (1.4×10^{-15}), R_i is the reduction factor and f_i is the fractional coverage of i type of vegetation in a model grid (considering that vegetation cover can reduce dust emissions). u^* and u_{*t} are the friction and threshold friction velocities. RH and RHt are the relative humidity and threshold relative humidity near the surface. The total dust emission flux is apportioned to each size bin based on field measurements of vertical dust flux size distribution s in Chinese deserts.

Line 377: Why was this averaging done?

Response: Observations from a large number of stations are being used for meteorological comparisons. It is hard to show site-by-site comparison, so we use averaged and stand deviation to show spatial variations. Site-by-site comparisons were done in our previous papers focusing on the North China Plain, and the results show similar conclusions as this study: temperature and water vapor are simulated well, but wind speeds are overestimated during haze periods (Gao et al., 2016a).

Gao, M., et al. (2016a). "Modeling study of the 2010 regional haze event in the North China Plain." *Atmospheric Chemistry and Physics* 16(3): 1673-1691.

Lines 462-463: Are the high values of the liquid water path simulated by M6 over Northern China really realistic? It looks like almost cloudless conditions are simulated by all the other models. What is the reason for these extremely high values of the LWP simulated by M6?

Response: They might not be realistic. The cumulus cloud physics and microphysics used by M6 are outdated and different from other models (Grell 3D was used by all other models), which might be the reason for different predictions of liquid water path.

Line 463: Please explain the reason for the poor performance of M7?

Response: The results shown for M7 is from simulation that aerosol-radiation was not turned on (offline), so M7 radiation are higher than other models. We add this information in the revised manuscript "Online coupled WRF-CMAQ only considers aerosol-radiation interactions but no aerosol indirect effects. The WRF-CMAQ results shown in this paper are from an offline simulation (aerosol-radiation interaction was turned off)."

"The slightly higher daily maximum SWDOWN from M7 than other models is due to the deactivation of aerosol-radiation interactions in the presented M7 simulation."

The online results of WRF-CMAQ will be presented in the companion paper part II.

Lines 518-544 and response to reviewer #2: Not all reviewer comments are addressed in the revised version and in the response. Still no proper explanation is given for high ozone concentrations simulated by M4 and M4. Also, it is not discussed whether this difference is related to the maximum values or whether the concentrations during nighttime are not well reproduced. Neither the revised text nor the response to the reviewer gives an answer to this question. The attempt of an explanation, i.e. larger vertical diffusion, which results in less titration of ozone by NO, cannot really explain the higher ozone concentrations since the NO_x concentrations simulated by M3 and M4 are quite similar to the concentrations found for M1. The authors might carefully check whether the implementation of RADM2 into NU-WRF is identical to the implementation of RADM2 with chem opt=1 into WRF-Chem. If this is the case, then titration of ozone by NO_x is underestimated for regions with high NO_x (see Forkel et al., 2015, see Figure S1 and the Appendix of that paper). However, this explanation must not be adopted uncritically by the authors – it is only valid if NU-WRF uses the same solver for RADM2 as it is used for chem_opt=1 in WRF-Chem!

Response: Thanks for these good suggestions. We checked the results that the difference is related to the too high concentrations during nighttime. We have confirmed with the NASA modeling group that the implementation of RADM2 in NU-WRF is identical to it in WRF-Chem. They just used the same codes in WRF-Chem v3.5.1 package: module_data_radm2.F and module_radm.F. In East China, where NO_x concentrations are even higher than in Europe (Forkel et al., 2015), so this is the main reason for overestimation of ozone in M3 and M4. We have added these explanations in the revised manuscript: "The overestimations of ozone concentrations from M3 and M4 primarily occur during nighttime, implying the underestimated titration

of ozone by NO_x. Forkel et al. (2015) reported that the RADM2 solver in WRF-Chem has the problem of underestimating ozone titration in areas with high NO emissions, which is the version that applied in M3 and M4.”

Line 647: The reference Zhao et al. (2015) is missing

Response: We add the following one:

Zhao, B., Wang, S., Donahue, N.M., Jathar, S.H., Huang, X., Wu, W., Hao, J. and Robinson, A.L., 2016. Quantifying the effect of organic aerosol aging and intermediate-volatility emissions on regional-scale aerosol pollution in China. Scientific reports, 6, p.28815.

Line 670: Compositions cannot be high. Please reword

Response: Thanks for pointing out. We add “mean concentrations of” before “PM_{2.5} chemical compositions”.

Lines 693 – 698: Are these small differences in the correlation coefficient really relevant?

Response: Thanks for pointing out. We delete these sentences of correlation coefficient.

Lines 717 – 725: All the mentioned concentrations are near surface values whereas AOD reflects vertically integrated values. Please add some comment about this issue.

Response: Thanks for this great suggestion. We change the sentence to “which can partially explain the largest simulated AOD by M2” and add another comment “The largest simulated AOD by M2 could also be related to different vertical distributions of aerosols”.

Lines 782 – 783: This is just a rather general statement. The role of deposition is not discussed in more detail earlier in the paper.

Response: We delete this sentence in the revised manuscript.

Table 1: 1) Does ‘Not available’ mean ‘not considered in the simulation’ or just ‘not supplied’? 2) What is the meaning of the blank spaces in the table (microphysics and surface physics for WRF-CMAQ)?

Response: NA means not considered in the simulation here. I add this description under the Table. I fill in the blank spaces in the revised manuscript.

Caption of Figure 1: ‘M6’ and ‘M7’ is missing before RegCCMs and WRF-CMAQ, respectively.

Response: We add ‘M6’ and ‘M7’.

Indicating the locations of those stations where results are shown in the paper or in the supplement in Figures 6 and 7 would be helpful.

Response: We have added names of those stations in Figure S6 and S7.

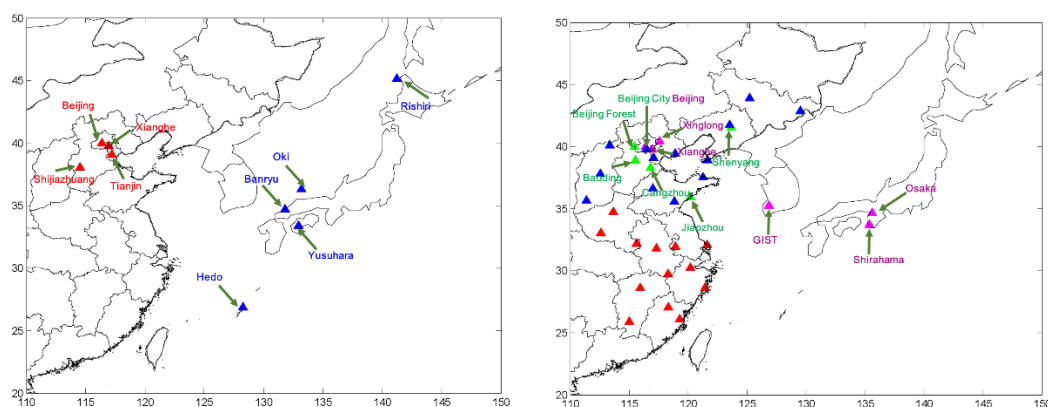


Figure S9 (and related text): The absence of aerosol cloud interactions does not necessarily mean that no cloud water is simulated. So, why is the liquid water path not shown for M7?

Response: M7 did not submit liquid water path results, but it would be similar to M1 and M2.

Caption of Figure S10: According to the text of the paper, the curves show M2.

Response: Thanks for pointing out. We have changed it to M2.

Response to reviewer #2: The explanations about wind-blown dust should also be included in the paper.

Response: We add descriptions of dust emissions in subsection 2.2.6 and include the responses to reviewer #2 in the paper: “In winter of the North China Plain, soil dust generally contributes about 10% to PM_{2.5} concentrations (He et al., 2014), but there is also primary PM from anthropogenic activity, such as power plant, traffic, and construction etc. The primary particles are mostly in coarse mode, which might contribute to PM₁₀ concentrations, but are highly uncertain compared with other anthropogenic emission sectors”.

In addition, we add the following discussions about wind-blown desert dust: “The spatial distributions of predicted wind-blown dust from M5 are slightly different from M2 and M3, with lower concentrations over the Gobi desert (in west Inner Mongolia) (PM₁₀ in Figure 8). M2 and M3 used similar GOCART dust emission schemes based on wind speeds and erodible areas, while M5 furtherly considered the dust reduction by vegetation cover, which could partially explain the relatively lower wind-blown dust predictions from M5”.

Final question: What is the status of the companion papers? Please add some more information (first author, journal).

Response: We are still analyzing the model outputs for the companion papers. The authors would be the similar to those in this manuscript, and would be published in the same special issue in ACP. We will further discuss about the model results and paper writing in a workshop to be held in next month and the companion paper will be submitted soon in one or two months.

**Air Quality and Climate Change, Topic 3 of the Model Inter-Comparison
Study for Asia Phase III (MICS-Asia III), Part I: overview and model
evaluation**

Meng Gao^{1,2}, Zhiwei Han^{3,4}, Zirui Liu⁵, Meng Li^{6, ~~43~~7}, Jinyuan Xin⁵, Zhining ~~Tao~~⁷Tao^{8,82}, Jiawei Li^{3,4},
Jeong-Eon ~~Kang~~⁹Kang¹⁰, Kan ~~Huang~~¹⁰Huang¹¹, Xinyi ~~Dong~~¹⁰Dong¹¹, Bingliang ~~Zhuang~~¹¹Zhuang¹², Shu
~~Li~~¹¹Li¹², Baozhu Ge⁵, Qizhong ~~Wu~~¹²Wu¹³, Yafang ~~Cheng~~¹³Cheng⁷, Yuesi Wang⁵, Hyo-Jung ~~Lee~~⁹Lee¹⁰,
Cheol-Hee ~~Kim~~⁹Kim¹⁰, Joshua S. ~~Fu~~¹⁰Fu¹¹, Tijian ~~Wang~~¹¹Wang¹², Mian ~~Chin~~⁸Chin⁹, Jung-Hun Woo¹⁴,
Qiang Zhang⁶, Zifa Wang^{4,5}, Gregory R. Carmichael¹

1 Center for Global and Regional Environmental Research, University of Iowa, Iowa City, IA, USA

2 John A. Paulson School of Engineering and Applied Sciences, Harvard University, Cambridge, MA, USA

3 Key Laboratory of Regional Climate-Environment for Temperate East Asia, Institute of Atmospheric Physics,
Chinese Academy of Sciences, Beijing, China

4 University of Chinese Academy of Sciences, Beijing 100049, China

5 State Key Laboratory of Atmospheric Boundary Layer Physics and Atmospheric Chemistry, Institute of
Atmospheric Physics, Chinese Academy of Sciences, Beijing, China

6 Ministry of Education Key Laboratory for Earth System Modeling, Center for Earth System Science, Tsinghua
University, Beijing, China

~~43~~7 [Multiphase Chemistry Department, Max Planck Institute for Chemistry, Mainz, Germany](#)

~~7~~8 Universities Space Research Association, Columbia, MD, USA

~~8~~9 NASA Goddard Space Flight Center, Greenbelt, MD, USA

22 ~~9-10~~ Department of Atmospheric Sciences, Pusan National University, Busan, South Korea
23 ~~11~~ Department of Civil and Environmental Engineering, University of Tennessee, Knoxville, TN, USA
24 ~~12~~ School of Atmospheric Sciences, Nanjing University, Nanjing, China
25 ~~13~~ College of Global Change and Earth System Science, Beijing Normal University, Beijing, China
26 ~~13~~ Multiphase Chemistry Department, Max Planck Institute for Chemistry, Mainz, Germany
27 14 Department of Advanced Technology Fusion, Konkuk University, Seoul, South Korea
28 Correspondence to: M. Gao (mgao2@seas.harvard.edu), Z. Han (hzw@mail.iap.ac.cn), and G. R.
29 Carmichael (gcarmich@engineering.uiowa.edu)
30
31

32 Abstract

33 Topic 3 of the Model Inter-Comparison Study for Asia (MICS-Asia) Phase III examines how
34 online coupled air quality models perform in simulating high aerosol pollution in the North
35 China Plain region during wintertime haze events and evaluates the importance of aerosol
36 radiative and microphysical feedbacks. A comprehensive overview of the MICS-ASIA III Topic
37 3 study design, including descriptions of participating models and model inputs, the experimental
38 designs, and results of model evaluation, are presented. Six modeling groups from China, Korea
39 and the United States submitted results from seven applications of online coupled chemistry-
40 meteorology models. Results are compared to meteorology and air quality measurements,
41 including [data from](#) the Campaign on Atmospheric Aerosol Research Network of China (CARE-
42 China) network, and the Acid Deposition Monitoring Network in East Asia (EANET). The

correlation coefficients between multi-model ensemble mean and the CARE-China observed near-surface air pollutants range from 0.51 to 0.94 (0.51 for ozone and 0.94 for PM_{2.5}) for January 2010. However, large discrepancies exist between simulated aerosol chemical compositions from different models, ~~which is due to different parameterizations of chemical reactions~~. The coefficient of variation (standard deviation divided by the mean) can reach above 1.3 for sulfate in Beijing, and above 1.6 for nitrate and organic aerosols in coastal regions, indicating these compositions are less consistent from different models. During clean periods, simulated Aerosol Optical Depths (AOD) from different models are similar, but peak values differ during severe haze events, which can be explained by the differences in simulated inorganic aerosol concentrations and the hygroscopic growth efficiency (affected by varied relative humidity). These differences in composition and AOD suggest that future models can be improved by including results present how current online-coupled meteorology-chemistry models reproduce severe haze events, and provide some directions for future model improvements, such as new heterogeneous or aqueous pathways for sulfate and nitrate formation under hazy conditions, secondary organic aerosol (SOA) formation chemical mechanism with new volatile organic compounds (VOCs) precursors, yield data and approaches, and more detailed evaluation of the dependence of aerosol optical properties on size distribution and mixing state. It was also found that using the ensemble mean of the models produced the best prediction skill. While this has been shown for other conditions (for example prediction of high ozone events in the US (McKeen et al., 2004), this is to our knowledge the first time it has been shown for heavy haze events.

1 Introduction

Air pollution in Asia, particularly in China and India, has been an increasingly important research topic, and has attracted enormous media coverage since about 60% of the world population live and are exposed to extremely unhealthy air in this region. It is estimated that outdoor air pollution brings about 3.3 million premature deaths per year worldwide with most deaths occurring primarily in Asia (Lelieveld et al., 2015). In addition, the impacts of regional and intercontinental transport of Asian pollutants on air quality and climate change have been frequently reported (Akimoto, 2003; Menon et al., 2002; Ramanathan and Carmichael, 2008). Chemical transport models have been developed and applied to study various air pollution issues in Asia. For example, an Eulerian regional scale acid deposition and photochemical oxidant model was developed in the United States (Carmichael and Peters, 1984; Carmichael et al., 1986; Carmichael et al., 1991) and applied to study long-range transport of sulfur oxides (SO_x), dust and ozone production in East Asia (Carmichael et al., 1998; Xiao et al., 1997). A nested urban and regional scale air quality prediction modeling system was developed and applied to investigate ozone pollution in Taiwan (Wang et al., 2001). Although important advances have taken place in air quality modeling, large uncertainties still remain, which are related to inaccurate and/or incomplete emission inventories, poorly represented initial and boundary conditions and missing or poorly parameterized physical and chemical processes (Carmichael et al., 2008a).

Furthermore, many models used to study air quality in Asia ~~have been~~ were developed in other regions (e.g., USA and Europe), and the assumptions and parameterizations included in these models may not be applicable to the Asian environment. In order to develop a common

87 understanding of model performance and uncertainties in Asia, and to further develop the models
88 for Asian applications, a model inter-comparison study was initiated, i.e., Model Inter-
89 Comparison Study for Asia Phase I (MICS-Asia I), in 1998 during a workshop on Transport of
90 Air Pollutants in Asia in Austria. The focus of MICS-Asia Phase I was to study long-range
91 transport and deposition of sulfur within Asia in support of on-going acid deposition studies.
92 Eight long-range transport models from six institutes in Korea, Japan, Denmark, the USA, and
93 Sweden participated in MICS-Asia I. Multi-model results of sulfur dioxide (SO₂) and sulfate
94 concentrations, and wet deposition amounts in January and May 1993 were compared with
95 surface observations in East Asia (Carmichael et al., 2002). Source-receptor relationships and
96 how model structure and parameters affect model performance were also discussed during this
97 phase (Carmichael et al., 2002). In 2003, MICS-Asia Phase II was initiated to include more
98 species, including nitrogen compounds, ozone and aerosols. The study period was expanded to
99 cover two different years and three different seasons, and global inflow to the study domain was
100 also considered (Carmichael et al., 2008b). Nine modeling groups from Korea, Hong Kong,
101 Japan, the USA, Sweden, and France participated in this phase. Seven topics (i.e., ozone and
102 related precursors, aerosols, acid deposition, global inflow of pollutants and precursors to Asia,
103 model sensitivities to aerosol parameterization, analysis of emission fields, and detailed analyses
104 of individual models) were discussed and published in a special issue of Atmospheric
105 Environment (Carmichael et al., 2008b).

106 In 2010, MICS-Asia phase III was launched and three topics for this phase were decided during
107 the first and second Workshop on Atmospheric Modeling in East Asia. Phase III aims to evaluate
108 strengths and weaknesses of current air quality models and provide techniques to reduce
109 uncertainty in Asia (Topic 1), to develop a reliable anthropogenic emission inventory in Asia

110 (Topic 2), and to evaluate aerosol-weather-climate interactions (Topic 3). Various multi-scale
111 models participated in this phase, and the study periods range from year to month depending on
112 study topics. This phase ~~benefits from~~~~uses data from~~ the Acid Deposition Monitoring Network in
113 East Asia (EANET) measurements, in addition to new observations related to atmospheric
114 chemistry in ~~the~~this region. A detailed overview of the MICS-Asia Phase III, including the
115 descriptions of different research topics and participating models, will be published in a
116 companion paper. An important advance to this phase is the inclusion of multiple online-coupled
117 chemistry-meteorology models to investigate aerosol-weather-climate interactions, which is the
118 target of topic 3. On-line coupled models are playing important roles in air quality, meteorology
119 and climate applications, but many important research questions remain (Baklanov et al., 2017).

120 The influences of aerosols on meteorology, e.g., radiation, temperature, boundary layer heights,
121 winds, etc. and PM_{2.5} concentrations have been examined in previous studies using different
122 online coupled models (Forkel et al., 2015; Gao et al., 2016a, 2016b, 2017a, 2017b; Han et al.,
123 2012, 2013; Makar et al., 2015a, 2015b; San Jose et al., 2015; Tao et al., 2015, 2016; Wang et
124 al., 2014; Zhang et al., 2010). In general, there are two ways of online coupling: online integrated
125 coupling (meteorology and chemistry are simulated using the same model grid, and one main
126 time step is used to integrate) and online access coupling (meteorology and chemistry are
127 independent but data are exchanged on a regular basis) (Baklanov et al., 2014). These two
128 different coupling ways can lead to uncertainties in the results of aerosol-weather-climate
129 interactions. Even using the same coupling way, different parameterizations in different online
130 models causes uncertainties as well. Thus, it is important to inter-compare how different online
131 models simulate aerosol-weather-climate interactions, particularly in heavily polluted Asian
132 region. Other ongoing related modeling frameworks include the Task Force on Hemispheric

133 Transport of Air Pollution (TF HTAP) and the Air Quality Model Evaluation International
134 Initiative (AQMEII). The TF HTAP was initiated to improve knowledge of the intercontinental
135 or hemispheric transport and formation of air pollution, and its impacts on climate, ecosystems
136 and human health (Galmarini et al., 2017; Huang et al., 2017). The AQMEII project specifically
137 focuses on regional modeling domains over Europe and North America (Galmarini et al., 2017),
138 within which aerosol meteorology interactions ~~was-were~~ studied (Forkel et al., 2015; Makar et
139 al., 2015a, 2015b; San Jose et al., 2015) over Europe and North America.

140 This paper ~~presents and overview~~s of the MICS-ASIA III Topic 3, serving as the main repository
141 of the information linked to Topic 3 simulations and comparisons. Specifically, this paper aims
142 to archive the information of the participating models, how the experiments are designed, and the
143 results of model evaluation. The results of the MICS-Asia Topic 3 experiments looking at the
144 direct and indirect effects during heavy haze events will be published in a companion paper, part
145 II. ~~This paper is organized as follows: i~~In Section 2, we provide the inter-comparison framework
146 of Topic 3, including the participating models, emissions, boundary conditions, observational
147 data, and analysis methodology. Section 3 ~~presents the general descriptions of the study periods~~
148 ~~and Section 4~~ presents comparisons and discussions focused on the results related to the
149 meteorological and air pollution conditions during the January 2010 heavy haze episode. ~~The~~
150 ~~results of January 2013 haze episode and detailed analysis of the direct and indirect effects will~~
151 ~~be presented in a companion paper.~~

152

153 2 Inter-comparison framework

In North China, severe aerosol pollution frequently happens and attracts enormous interests from both ~~the~~ public and ~~the~~ scientific ~~communities-community~~ (Cheng et al., 2016; Gao et al., 2015, 2016a, 2016b, 2016c). Two winter months in which severe haze episodes happened in North China were selected as the study periods for Topic 3. During these two months, maximum hourly PM_{2.5} concentration in urban Beijing reached ~500 µg/m³ and 1000µg/m³, respectively. Compared to the China Grade 1 24-h PM_{2.5} standard (35µg/m³), daily mean PM_{2.5} concentrations in urban Beijing exceeded this standard ~~for-on~~ 20 days and 27 days within these two months, respectively. The dramatically high aerosol loadings during these two hazy months substantially affected radiation transfer, and provide a good opportunity to study the aerosol effects on weather, air quality and climate. In this study, the participants were required to use common emissions to ~~predict-simulate~~ air quality during these two months and submit requested model variables. The emissions were placed on a publicly accessible website. Six modeling groups submitted results for Topic 3. In this section, we briefly describe these models and their configurations, introduce the emission inventories (including anthropogenic, biogenic, biomass burning, air and ship, and volcano emissions) ~~and the~~ -observational datasets, and ~~describe~~ ~~present~~ the analysis methodology.

2.1 Participating models

Table 1 summarizes the characteristics of the participating models. These models include: one application of the Weather Research Forecasting model coupled with Chemistry (WRF-Chem, Fast et al., 2006; Grell et al., 2005) by Pusan National University (PNU) (M1), one application of the WRF-Chem model by the University of Iowa (UIOWA) (M2), two applications (two domains: 45km and 15km horizontal resolutions) of the National Aeronautics and Space Administration (NASA) Unified WRF (NU-WRF, Peters-Lidard et al., 2015; Tao et al., 2013)

177 model by the Universities Space Research Association (USRA) and NASA's Goddard Space
178 Flight Center (M3 and M4), one application of the Regional Integrated Environment Modeling
179 System with Chemistry (RIEMS-Chem, Han et al., 2010) by the Institute of Atmospheric Physics
180 (IAP), Chinese Academy of Sciences (M5), one application of the coupled Regional Climate
181 Chemistry Modeling System (RegCCMS, Wang et al., 2010) from Nanjing University (M6), and
182 one application of the coupled WRF-CMAQ (Community Multiscale Air Quality) model by the
183 University of Tennessee at Knoxville (UTK) (M7). These models are all online coupled, which
184 enables aerosol-weather-climate interactions. Domain setting of each model application is shown
185 in Figure 1. The domains of M2, M5, and M6 (UIOWA, IAP, and NJU in Figure 1) cover most
186 areas of East Asia, including China, North Korea, South Korea, Japan, Mongolia, and northern
187 parts-region of Southeast Asia. M1, M3 and M7 domains (PNU, NASA D01 and UTK) include
188 more countries in Southeast and South Asia. M4 (NASA D02) covers east China, Korea and
189 Japan. The descriptions of major model settings are listed below. More descriptions including
190 microphysics, radiation, and boundary layer, are listed in Table 1.

191 (1) Model grids: The horizontal model resolutions of these applications range from 15km to
192 60km (Table 1). Model vertical resolutions vary from 16 to 60 layers (Table 1) and the set model
193 top pressures range from 100mb to 20mb (Table 1).

194 (2) Gas phase chemistry: At PNU (M1), the RACM-ESRL (Regional Atmospheric Chemistry
195 Mechanism, [Stockwell et al., 1997](#), Earth System Research Laboratory, [Kim et al., 2009](#)) gas
196 phase chemistry was used. RACM was developed based on [the](#) Regional Acid Deposition Model
197 (RADM2) to simulate regional atmospheric chemistry (Stockwell et al., ~~1997~~1990) (including
198 237 reactions) and the rate coefficients were updated in [the](#) RACM ESRL version (Kim et al.,
199 2009). At the University of Iowa (M2), CBMZ (Carbon-Bond Mechanism version Z) gas phase

200 chemistry was used. CBMZ (Zaveri and Peters, 1999) extends the original CBM4 mechanism to
201 function properly at larger spatial and longer timescales. The augmented CBMZ scheme includes
202 67 species and 164 reactions. The NU-WRF model (M3 and M4) ~~uses-used~~ RADM2 for gas
203 phase chemistry. Both the RIEMS-Chem model from IAP (M5) and the RegCCMS model from
204 NJU (M6) ~~used~~ CBM4 to calculate gas phase chemistry (Gery et al., 1989). The CBM4 version
205 incorporated in RIEMS-Chem (M5) includes 37 species and 91 reactions. The version of CBM4
206 implemented in RegCCMS (M6) consists of 36 reactions (4 photolysis reactions) and 20 species
207 (Wang et al., 2010). M7 applied the SAPRC-99 mechanism to simulate gas phase chemistry. The
208 SAPRC99 mechanism implanted within the CMAQ model has 88 species and 213 chemical
209 reactions (Carter, 2000a, b).

210 (3) Aerosol modules: MADE/SORGAM (Modal Aerosol Dynamics Model for
211 Europe/Secondary Organic Aerosol Model, Ackermann et al., 1998) aerosol module ~~was~~
212 coupled by Schell et al. (2001) ~~and was~~ used in M1. MADE ~~usesuses~~ 3 log-normal modes
213 (Aitken, accumulation, coarse) and simulates major aerosol compositions, including sulfate,
214 ammonium, nitrate, sea-salt, black carbon (BC), and organic carbon (OC). M2 ~~uses-used an~~ 8 bin
215 MOSAIC (Model for Simulating Aerosol Interactions and Chemistry) aerosol module. MOSAIC
216 considers major aerosol species at urban, regional and global scales, including sulfate, nitrate,
217 ammonium, sodium, chloride, ~~ECBC~~, and other unspecified inorganic species (such as inert
218 minerals, trace metals, and silica) (Zaveri et al. 2008). The MOSAIC version used in M2
219 includes some aqueous reactions but no SOA formation. At NASA, the GOCART aerosol model
220 (Chin et al., 2002) was coupled to RADM2 gas phase chemistry, and incorporated into the NU-
221 WRF model (M3 and M4) to simulate major tropospheric aerosol species, including sulfate, BC,
222 OC, dust, and sea-salt. In this aerosol model, 10% of organic compounds from the volatile

organic compounds (VOCs) emission inventory ~~are-were~~ assumed to be converted to SOA (Chin et al., 2002). Aerosols in RIEMS-Chem include sulfate, nitrate, ammonium, BC, OC, SOA, 5 bins of soil dust, and 5 bins of sea salt (Han et al., 2012). ISORROPIA (Nenes et al., 1998) ~~is~~ was coupled to RIEMS-Chem to treat thermodynamic equilibrium process and to simulate inorganic aerosols. SOA production from primary anthropogenic and biogenic VOCs is calculated using a bulk aerosol yield method according to Lack et al. (2004). RegCCMS also used ISORROPIA to calculate inorganic aerosols (Wang et al., 2010). For implementation of aerosol effects, sulfate radiative properties were treated following Kiehl and Briegleb (1993), OC ~~aerosols were-are~~ assumed to have the same properties as sulfate, and the wavelength-dependent radiative properties of BC ~~follows-follows~~ Jacobson (2001). AE6 aerosol (the sixth-generation CMAQ aerosol module, Carlton et al., 2010) mechanism ~~is-was~~ coupled with WRF. Compared to previous version of CMAQ aerosol modules, AE6 improves SOA treatments, ~~adds-adds~~ a new heterogeneous N₂O₅ hydrolysis parameterization and ~~ads-adds~~ a new gas-to-particle mass transfer for coarse aerosols in sea-salt emissions (Yu et al., 2014). There are seven components, including water soluble mass, water insoluble mass, elemental carbon, sea salt, water, diameters and standard deviations, passed to WRF to directly change radiation calculations.

(4) Meteorological boundary and initial conditions: M1, M2, M5 and M7 used d the National Centers for Environmental Prediction (NCEP) final analysis (FNL) data to drive the model; M3 and M4 used d NASA MERRA reanalysis data and M6 ~~uses-used~~ NCEP-NCAR reanalysis 1 dataset (Kalnay et al., 1996).

(5) Soil dust: M1, M6 and M7 ~~do-did~~ not include soil dust calculation. M3 and M4 used d GOCART dust module (Ginoux et al., 2001), and M2 ~~uses-used~~ a GOCART version that

modified by AFWA (Air Force Weather Agency). M5 ~~uses-used~~ a dust module that described in Han et al. (2004).

(6) Mixing state: M6 assumes external mixing, while other models use internal mixing treatments for major aerosol compositions.

Many previous studies have underscored that the choice of gas phase mechanism and aerosol models are of great importance for simulating air pollutants (Knote et al., 2015). The different gas phase chemistry and aerosol modules used in the participating models are expected to yield notable differences in performances, which are shown later in section 4.3.

2.2 Emissions

The accuracy of air quality modeling results highly depends on the quality and reliability of emission inventory. Accordingly, a new Asian emission inventory was developed for MICS-III by integrating state-of-the-art national/regional inventories to support this model inter-comparison study (Li et al., 2017). This is the major theme of MICS-ASIA III Topic 2. These emissions, along with biogenic emissions, biomass burning emissions, emissions from air and ship transport, ~~and~~ volcano emissions, and dust emissions were used. This section ~~offers-provides~~ some basic descriptions of these ~~provided~~ emissions.

2.2.1 Anthropogenic emissions

The state-of-the-art anthropogenic emission inventory for Asia (MIX) was developed by incorporating five inventories, including the REAS inventory for Asia developed at the Japan National Institute for Environmental Studies (NIES), the MEIC inventory for China developed at Tsinghua University, the high resolution ammonia (NH₃) emission inventory in China developed

at Peking University, the Indian emission inventory developed at Argonne National Laboratory in the United States, and the CAPSS Korean emission inventory developed at Konkuk University (Li et al., 2017). This MIX inventory includes emissions for ten species, namely SO₂, nitrogen oxides (NO_x), carbon monoxide (CO), non-methane volatile organic compounds (NMVOC), NH₃, PM₁₀, PM_{2.5}, BC, OC, and carbon dioxide (CO₂). NMVOC ~~are~~ were provided with CB-05 and SAPRC-99 speciation datasets. Speciation mapping of NMVOC emissions for groups using other gas-phase chemical mechanisms, such as CBMZ, RADM2 and CBM4, used the speciation framework documented in Li et al. (2014). Emissions of these species were prepared for years 2008 and 2010 with a ~~in~~ monthly temporal resolution and 0.25 degree spatial resolution. Weekly/diurnal profiles were also provided. Five sectors were considered, namely industry, power generation, residential sources, transportation and agriculture. Figure 2 shows the spatial maps of these ten species for January 2010. Emissions of most of these species exhibit similar spatial patterns, with enhanced values in east China and lower values in north and south India. Emissions of NH₃ display a different spatial distribution, with pronounced values in India and lower values in north China (Figure 2). More detailed description of this emission inventory is documented in Li et al. (2017).

2.2.2 Biogenic emissions

Terrestrial ecosystems generate various chemical species, including volatile and semi-volatile compounds, which play important roles in atmospheric chemistry and are the largest contributor to global annual flux of reactive volatile organic compounds (VOCs) (Guenther et al., 2006). For MICS-ASIA III, hourly biogenic emissions were provided for the entire year of 2010 using the Model of Emissions of Gases and Aerosols from Nature (MEGAN) version 2.04 (Guenther et al., 2006). The variables that drive MEGAN include land cover information (plant function type, leaf

area index) and weather conditions, which includes solar transmission, air temperature, humidity, wind speed, and soil moisture. In the preparation of MEGAN biogenic emissions, land cover information ~~is was~~ taken from the NASA MODIS products, and weather conditions ~~are were~~ calculated using ~~the~~ WRF simulations. Figure S1 shows biogenic emissions of some selected species (isoprene and HCHO) for January 2010. High biogenic emissions are found in south Asia during winter, including India, south China, and Southeast Asia, where solar radiation, air temperature and vegetation covers are relatively higher than in northern regions. As shown in Table 1, M1 and M5 used ~~d~~ prescribed biogenic VOCs emissions, other models except M6 used ~~d~~ internal calculation.

2.2.3 Biomass burning emissions

Biomass burning ~~in the tropics~~ is a strong contributor to air pollutants, and extensive biomass burning in Asia, particularly Southeast Asia, exerts a great influence on air quality (Streets et al., 2003). For MICS-ASIA III, biomass burning emissions were processed by re-gridding the Global Fire Emissions Database version 3 (GFEDv3, [Randerson et al., 2015](#)) (0.5 by 0.5 degree). GFED fire emissions are estimated through combining satellite-detected fire activity and vegetation productivity information. Carbon, dry matter, CO₂, CO, CH₄, hydrogen, nitrous oxide, NO_x, NMHC, OC, BC, PM_{2.5}, total particulate matter and SO₂ emissions are estimated ~~in with~~ monthly temporal resolution. Figure S2 shows the gridded biomass burning emissions for January 2010. Biomass burning activity ~~is was~~ highest in Cambodia and some areas of Myanmar and north of Thailand (Figure S2), and the peak emission season is spring. Although it has been concluded that biomass burning could significantly contribute to aerosol concentrations in China, the contribution is limited for Topic 3 study since the focused region is North China where biomass burning emissions are negligible during winter (Gao et al., 2016a).

312 2.2.4 Volcanic SO₂ emissions

313 Volcanoes are important sources of various sulfur and halogen compounds, which play crucial
314 roles in tropospheric and stratospheric chemistry. It is estimated that SO₂ emitted from volcanoes
315 account for about 9% of the total worldwide annual SO₂ flux (Stoiber et al., 1987). The Asia-
316 Pacific region is one of the most geologically unstable regions in the world where many active
317 volcanoes are located. During MICS-ASIA Phase II, the volcano SO₂ emissions had already
318 been provided for chemical transport models (Carmichael et al. 2008b). Volcano SO₂ emissions
319 were provided, with a daily temporal resolution. In January, some volcanoes in Japan are very
320 active, such as Miyakejima (139.53°E, 34.08°N, and 775m above sea level) and Sakurajima
321 (130.65°E, 31.59°N, 1117m above sea level).

322 2.2.5 Air and Ship emissions

323 Fuel burning in aircraft and ship engines produces greenhouse gases and air pollutants. The
324 shipping and aircraft emissions used are based on the HTAPv2 emission inventory (0.1 by 0.1
325 degree) for year 2010 (Janssens-Maenhout et al., 2015), provided on an annual basis. Aircraft
326 emissions include three parts: landing and takeoff (LTO), climbing and descent (CDS), and
327 cruise (CRS). Aircraft emission hot spots are mostly located in Japan, and Beijing, Yangtze
328 River Delta (YRD) and Pearl River Delta (PRD) in China (Figure S3). East China Sea, sea
329 around Japan and Singapore exhibit high shipping emissions due to active shipping
330 transportation (Figure S3). It is estimated that international shipping contributed about 10% to
331 the global SO₂ emissions, and together with aviation contribute more than 10% ~~of to~~ global NO_x
332 emissions (Janssens-Maenhout et al., 2015).

333 2.2.6 Dust emissions

Formatted: Font: Bold

In M2, the Air Force Weather Agency (AFWA) version of the GOCART dust model was used. It calculates the saltation flux as a function of friction velocity (u_*) and threshold friction velocity (u_{*t}):

$$Q = C \frac{\rho_0}{g} u_*^3 \left(1 + \frac{u_{*t}}{u_*}\right) \left(1 - \frac{u_{*t}^2}{u_*^2}\right) \text{ when } u_* \geq u_{*t}$$

where C is a tunable empirical constant, ρ_0 is air density, and g is gravitational acceleration. The bulk vertical dust flux is estimated by $F = \alpha QE$ (Marticorena and Bergametti, 1995), in which α is the sandblasting efficiency and E is the dust erodibility factor. The erodibility factor data is included in the model geography dataset.

In M3 and M4, the dust emissions are estimated using the GOCART dust model (Ginoux et al., 2001), which determined by soil texture, moisture and surface wind speed. The drier the soil and the stronger the wind, the higher dust emissions over the regions where the erodibility factor is not zero. In M5, soil dust emissions were estimated by the approach from Han et al. (2004):

$$F = C_0 u_*^4 \left(1 - \frac{u_{*t}}{u_*}\right) (1 - f_i R_i) \text{ when } u_* \geq u_{*t}, RH \leq RH_t$$

C_0 is a constant (1.4×10^{-15}), R_i is the reduction factor and f_i is the factional coverage of i type of vegetation in a model grid (considering that vegetation cover can reduce dust emissions). u_* and u_{*t} are the friction and threshold friction velocities. RH and RH_t are the relative humidity and threshold relative humidity near the surface. The total dust emission flux is apportioned to each size bin based on field measurements of vertical dust flux size distribution s in Chinese deserts.

2.3 Boundary conditions

To predict more realistic spatial and temporal variations of air pollutants, boundary conditions from global chemical transport models are necessary to drive regional chemical transport models (Carmichael et al., 2008b). Simulations of two global chemical transport models (i.g., GEOS-Chem and MOZART) were used as boundary conditions for MICS-ASIA III. GEOS-Chem was developed in the USA to simulate tropospheric chemistry driven by assimilated meteorology (Bey et al., 2001). The National Center for Atmospheric Research (NCAR) also provides global simulations of atmospheric chemistry (MOZART model) and an interface to convert them to WRF-Chem boundary conditions (Emmons et al., 2010), and NASA provides global aerosol distributions using the global GOCART chemistry model (Chin et al., 2002). GEOS-Chem was run with 2.5°x2° resolution and 47 vertical layers. The MOZART-4 simulations were configured at the horizontal resolution of 2.8°x2.8°, and with 28 vertical levels. NASA GOCART was configured at the same resolution as GEOS-5 meteorology (1.25°x1°). As listed in Table 1, M1 used climatological data from the NOAA Aeronomy Lab Regional Oxidant Model (NALROM), while M2 used boundary conditions from the MOZART-4 (provided from the NCAR website). M3 and M4 used MOZART-4 as boundary conditions for gases and used GOCART as boundary conditions for aerosols. M6 also used fixed climatology boundary conditions, and M5 and M7 used GEOS-Chem outputs as boundary conditions. The spatial distribution of near surface concentrations of major gases and aerosols from both GEOS-Chem and MOZART are shown in Figure S4. Even ~~though-if~~ the same global chemistry model is used as boundary conditions, the treatments of inputs might differ in details, which might lead to dissimilarities. In MICS-ASIA II, Holloway et al. (2008) discussed the impacts of uncertainties in global models on regional air quality simulations.

2.4 Observation data

378 Historically, the lack of reliable air quality measurements in Asia has been an ~~bottleneck-obstacle~~
379 in understanding air quality and constraining air quality modeling in Asia. Beginning with
380 MICS-ASIA II, observational data from ~~the~~ Acid Deposition Monitoring Network in East Asia
381 (EANET) has been used to evaluate model performance. EANET was launched in 1998 to
382 address acid deposition problems in East Asia, following the model of the Cooperative Program
383 for Monitoring and Evaluation of the Long-range Transmission of Air pollutants in Europe
384 (EMEP). As of 2010, there ~~are-were~~ 54 wet deposition sites and 46 dry deposition sites in ~~the~~ 13
385 participating countries. Quality assurance and quality control measures ~~are-were~~ implemented at
386 the national levels and in the Inter-laboratory Comparison Project schemes to guarantee high
387 quality dataset. EANET supported current activities of MICS-ASIA III, and provided
388 measurements in 2010 to all modeling groups. More information about ~~the~~ EANET dataset can
389 be found in <http://www.eanet.asia/>.

390 In addition to ~~the~~ EANET data, measurements of air pollutants and aerosol optical depth (AOD)
391 collected at the Campaign on Atmospheric Aerosol Research network of China (CARE-China)
392 (Xin et al., 2015) network were also used. Previous successful networks in Europe and the
393 United States underscored the importance of building comprehensive observational networks of
394 aerosols in China to get better understanding of the physical, chemical and optical properties of
395 atmospheric aerosols across China. As the first comprehensive attempt in China, CARE-China
396 was launched in 2011 by Chinese Academy of Sciences (CAS) (Xin et al., 2015). Before
397 launching this campaign, CAS had already been measuring air pollutants and AOD at some
398 CARE-China sites. Table 2 summaries the locations and characteristics of the CARE-China
399 measurements for January 2010. Air quality measurements include concentrations of PM_{2.5},
400 PM₁₀, SO₂, NO₂, NO, CO, O₃.

401 In addition, AOD from ~~the~~ Aerosol Robotic Network (AERONET)
402 (<https://aeronet.gsfc.nasa.gov/>) and ~~the~~ operational meteorological measurements (near surface
403 temperature, humidity, wind speed and downward shortwave radiation) in China and
404 atmospheric sounding data in Beijing were used. AERONET provides long-term, continuous,
405 readily accessible and globally distributed database of spectral AOD, inversion products and
406 precipitable water. AOD data are calculated for three quality levels: Level 1.0 (unscreened),
407 Level 1.5 (cloud screened), and Level 2.0 (cloud screened and quality assured) (Holben et al.,
408 1998). The locations and characteristics of the AERONET measurements are also summarized in
409 Table 2. In-situ measurements of meteorological data from standard stations in China are
410 operated by China Meteorological Administration (CMA) and different levels of data, including
411 daily, monthly, and annually, are open to the public (<http://data.cma.cn/en>). The locations of all
412 used observational sites are marked in Figure S5, Figure S6 and Figure S7.

413 The meteorology measurements (locations are shown in Figure S5) were averaged and compared
414 with model results ~~that averaged across those locations in pairs~~. The radiation measurements were
415 averaged and compared against model results in North China and South China (locations are
416 shown in Figure S6), separately. The CARE-China, AERONET and EANET measurements
417 (locations are shown in Figure S6 and S7) were compared against model results site by site, and
418 model ensemble mean values were ~~made-calculated~~ by averaging all model results.

419 2.5 Analysis methodology

420 All groups participating in Topic 3 were requested to simulate meteorology, air quality, radiative
421 forcing and effects of aerosols over the Beijing-Tianjin-Hebei region of east China during two

422 periods: January 2010 and January 2013. Each group was requested to submit the following
423 fields from their simulations.

424 (1) hourly mean meteorology:

425 (a) air temperature and water vapor mixing ratio at 2 ~~meters~~ above ground (T2, Q2), wind
426 speed at 10 ~~meters~~ above ground (WS10), and shortwave radiation flux (Wm^{-2}) at the surface;

Formatted: Superscript

427 (b) above variables (except shortwave radiation flux) at 1km and 3km above ground.

428 (2) hourly mean concentrations:

429 (a) SO₂, NO_x, CO, O₃, PM_{2.5}, PM₁₀ and sulfate, nitrate, ammonium, BC, OC and dust in PM_{2.5};

Formatted: Subscript

430 (b) above variables at 1km and 3km above ground.

431 (3) hourly mean aerosol optical depth (AOD), aerosol direct radiative forcings at the surface, top
432 of the atmosphere (TOA) and inside the atmosphere (single scattering albedo is an option for
433 participants).

434 (4) ~~Hourly~~ hourly mean integrated liquid water, cloud optical depth.

435 (5) Changes in T2, Q2, WS10 and PM_{2.5} concentrations at the surface due to both direct and
436 indirect aerosol's effects.

437 We calculated multiple model evaluation metrics, including correlation coefficient (r), root mean
438 square error (RMSE), mean bias error (MBE), normalized mean bias (NMB), mean fractional
439 bias (MFB) and mean fractional error (MFE). The equations for these metrics are presented in
440 supplemental information.

441

442 **3 General description of meteorology and haze during the study period**

443 Winter haze events frequently happen in east China, which is partially due to the stagnant
444 weather conditions in winter. Here we present general descriptions of the meteorological
445 conditions during January 2010 using the NCEP/NCAR reanalysis products. Figure S8 (a)
446 displays the monthly mean T2 (temperature at 2m) and W10 (wind speeds at 10m). WS10 were
447 very weak in eastern and central China regions, while lower T2 in Mongolia region was
448 associated with Siberian High. As shown in Figure S8 (b), the Siberian High center was about
449 1040mb, and there was no significant precipitation in North China and heavy rainfall only
450 occurred in Southeast Asia regions. During winters, northern China burns coal for heating,
451 generating more emissions. Under stagnant weather conditions, haze episodes are easily
452 triggered. High concentrations of aerosols during this month provide great opportunity to study
453 aerosol-radiation-weather interactions.

454

455 **4.3 Results and discussions**

456 Winter haze events frequently happen in east China, which is partially due to the stagnant
457 weather conditions in winter. Here we present general descriptions of the meteorological
458 conditions during January 2010 using the NCEP/NCAR reanalysis products. Figure S8 displays
459 the monthly mean T2 (temperature at 2 meters), WS10 (wind speeds at 10 meters) and total
460 precipitation. Near surface wind speeds were very weak in eastern and central China regions, and
461 there was no significant precipitation in North China (Figure S8). During winters, northern China

burns coal for heating, generating more emissions of air pollutants. Under stagnant weather conditions, haze episodes are easily triggered. High concentrations of aerosols during this month provide great opportunity to study aerosol-radiation-weather interactions.

In this section, we present some major features of model performances in meteorological and chemical variables for the January 2010 period. Detailed ~~analysis-analyses~~ of aerosol feedbacks and radiative forcing are presented in MICS-ASIA III companion papers. Heavy haze occurred over broad regions of East China in January 2010. The plots of observed meteorological variables and PM_{2.5} in Beijing show the general situation (Figure 3). Elevated PM_{2.5} occurred during three periods separated in time by roughly one week (January 8, 16 and 26). The major event occurred during January 15-21. The events occurred during periods of low wind speeds, and increasing temperature and relative humidity. The high PM_{2.5} concentrations during January 15-21 also greatly reduce the downward shortwave radiation. Below we evaluate how well the models predict these features.

4.3.1 Evaluation of meteorological variables

Air quality is affected by not only emissions, but also meteorological conditions. Meteorology affects air quality through altering emissions, chemical reactions, transport, turbulent mixing, and deposition processes (Gao et al., 2016c). Thus, it is important to assess how well these participating models reproduced meteorological variables. The predicted temperature at ~~2m-high~~ meters (T2), water vapor mixing ratio at ~~2m-2 meters~~ (Q2), wind speed at ~~10m-high meters~~ (WS10) and daily maximum downward shortwave radiation (SWDOWN) were evaluated against near surface observations at the CMA sites.

Figure 4 (a-c) shows the comparisons between simulated and observed daily mean T2, Q2 and WS10 averaged over stations in East China (locations are shown in Figure S5) during January 2010, along with multi-model ensemble mean and observational standard deviation. The calculated correlation coefficients between models and observations are also shown in Figure 5-4 and other calculated model evaluation metrics are summarized in Table 3. In general, the simulated magnitudes and temporal variations of T2 and Q2 show high order of consistencies with observations, with correlation coefficients ranging from 0.88 to 1. For T2, models tend to have a cool bias; M1 and M2 have the lowest RMSE (0.64 and 0.68), lowest MBE (-0.19 and -0.60) and lowest NMB (-0.07% and -0.22%) values (Table 3). For Q2, most models tend to slightly overestimate; M1 and M2 have the best performance, with the lowest RMSE (0.14 and 0.10), lowest MBE (0.02 and -0.01), and lowest NMB (0.84% and -0.55%) values (Table 3).

Simulated ~~WS10-wind speeds~~ exhibit larger diversity of results. All models tend to overestimate WS10, with MBE ranging from 0.15m/s to 2.37m/s. Overestimating wind speeds under low wind conditions is a common problem of current weather forecasting models, and many factors, including errors in terrain data and reanalysis data, relatively low horizontal and vertical model resolutions, as well as poorly parameterized urban surface effect, contribute to these overestimations. From the calculated RMSE, MBE, and NMB listed in Table 3, M2, M5 and M7 show better skills in capturing WS10. In addition, the multi-model ensemble mean show the lowest RMSE for Q2, and also better skills than most models for T2 and WS10. The correlation coefficients between multi-model ensemble mean and observations are 0.99, 0.99 and 0.98 for T2, Q2 and WS10, respectively.

The accuracy of radiation predictions is of great significance in evaluating aerosol-radiation-weather interactions. We evaluated simulated daily maximum SWDOWN averaged over sites in

506 northern China and southern China separately in January 2010 against observations. The
 507 locations of the radiation sites are shown in Figure S6. As shown in Figure 4 (d), over stations in
 508 northern China, all models except M6 and M7 reproduce daily maximum SWDOWN well, with
 509 correlation coefficients ranging from 0.72 to 0.94. The poor performance of M6 in North China
 510 is caused by largely overpredicted liquid water path (LWP) over North China (Figure S9). The
 511 slightly higher daily maximum SWDOWN from M7 than other models is due to the deactivation
 512 of aerosol-radiation interactions in the presented M7 simulation.
 513 SWDOWN decreases under conditions of high PM, as shown for example on January 9 and 15-
 514 21. This is one of the important reasons for coupled air quality and meteorology modeling, ~~as~~
 515 ~~they can account for this effect of aerosols.~~ It is worth noting that most models predict higher
 516 daily maximum SWDOWN compared to observations when severe haze happened in the North
 517 China Plain (16-19 January 2010), indicating aerosol effects on radiation might be
 518 underestimated. Besides, ~~c~~clouds are also important to alter radiation. To exclude ~~its clouds'~~
 519 impacts on the radiation shown here, we calculated the radiation reduction ratio ~~of radiation~~ due
 520 to clouds using radiation prediction for clear sky and ~~with clouds~~ for cloudy conditions from M2
 521 (shown in Figure S10). During the severe haze period (16-19 January 2010), the averaged
 522 reduction fraction is 5.9% in north China and 4.2% in south China, ~~suggesting~~ Thus, the
 523 relatively lower radiation during this period ~~shown in~~ (Figure 4(d)) is mainly caused by aerosols,
 524 ~~while but~~ the lowest radiation on 20 January was caused by clouds (Figure 4(d) and Figure S10).
 525 Over southern China sites (Figure 4e), M6 and M7 show a better consistence with observations
 526 than over northern China sites. According to the calculated RMSE listed in Table 3, M3 and
 527 multi-model ensemble mean exhibit relatively better performance in capturing the observed time
 528 series of daily maximum SWDOWN in both northern China and southern China.

The above comparisons show that T2 and Q2 ~~are-were~~ reproduced well by the participating models, ~~and-but WS10-is~~ wind speeds were overestimated by all models. Emery et al. (2001) proposed that excellent model performance would be classified as wind speed RMSE smaller than 2 m/s, and wind speed bias smaller than 0.5 m/s. Based on the calculated RMSE and MBE of WS10 shown in Table 3, RMSE values from all models match the proposed RMSE threshold but MBE values are higher than 0.5 m/s. The vertical distributions of temperature, water vapor mixing ratio and wind speeds were also validated against atmospheric sounding data in Beijing at 1km and 3km (Figure S11, averaged at 00:00 and 12:00 UTC) (<http://weather.uwyo.edu/upperair/sounding.html>). The magnitudes of temperature, water vapor mixing ratio and wind speeds from different models are generally consistent with each other at 1km and 3km, but variations are larger near the surface.

4.3.2 Evaluation of air pollutants

Figure 5 displays the daily averaged predicted and observed SO₂, NO_x, CO, O₃, PM_{2.5}, and PM₁₀ concentrations at the Beijing station, along with the observational standard deviation (locations are shown in Figure S7). Comparisons for the Tianjin, Shijiazhuang and Xianghe sites are shown in Figure S12-S14. M6 only provided SO₂, NO_x concentrations, so it is not shown in the plots of CO, O₃, PM_{2.5}, and PM₁₀. The observed and predicted ~~primary-primary gaseous~~ pollutants ~~and~~, PM_{2.5} and PM₁₀ show the same monthly variations with elevated values at roughly weekly intervals, with the largest event occurring during January 15-21. For example, as shown in the comparisons of SO₂ concentration, the temporal variations are reproduced well by all the models, but peak values are overestimated or underestimated by some models. Based on the calculated MBE values shown in Table 4, all models except M2 tend to underestimate SO₂ in the CARE-China sites. M1 shows the highest correlation (0.90) with SO₂ observations in the Beijing site,

552 and most other models show similar good correlations. The multi-model ensemble mean shows a
553 better agreement with observations with a higher correlation of 0.92, and it falls within the range
554 shown with standard deviation error bar. In general, the predictions for NO_x capture the main
555 features in the observations, with slightly less skills than for the SO₂ prediction. The calculated
556 correlation coefficients for NO_x from different models are close to each other, ranging from 0.63
557 to 0.88. M2 and M5 predict higher NO_x concentrations than observations and other models
558 (MBE in Table 4). All models overestimate NO_x concentration in Shijiazhuang (Figure S14),
559 suggesting NO_x emissions in Shijiazhuang might be overestimated in the MIX emission
560 inventory. All models produce similar CO predictions.

561 PM_{2.5} concentrations are well modelled, with high correlation coefficients ranging from 0.87 to
562 0.90 in Beijing, from 0.83 to 0.93 in Tianjin, and from 0.74 to 0.91 in Xianghe. The correlation
563 coefficient of the multi-model ensemble mean for PM_{2.5} reaches 0.94 (Table 4), better than any
564 individual model. The performances of all participating models in reproducing PM₁₀ variations
565 are not as good as reproducing PM_{2.5}. M1 and M2 overestimate PM₁₀ concentrations, and other
566 models underestimate PM₁₀ concentrations (MBE in Table 4). These biases are probably related
567 to different treatments of primary aerosols and anthropogenic dust in the models. In winter of the
568 North China Plain, soil dust generally contributes about 10% to PM_{2.5} concentrations (He et al.,
569 2014), but there is also primary PM from anthropogenic activity, such as power plant, traffic, and
570 construction etc. The primary particles are mostly in coarse mode, which might contribute to
571 PM₁₀ concentrations, but are highly uncertain compared with other anthropogenic emission
572 sectors.

573 The models showed the poorest skills in predicting ozone. All models exhibit different
574 performances in simulating ozone concentrations, and the correlation coefficients between

Formatted: Font: (Default) Times New Roman, 小四

Formatted: Font: (Default) Times New Roman, 小四

Formatted: Subscript

Formatted: Font: (Default) Times New Roman, 小四

Formatted: Font: (Default) Times New Roman, 小四

Formatted: Font: (Default) Times New Roman, 小四

Formatted: Font: (Default) Times New Roman, 小四

Formatted: Font: (Default) Times New Roman, 小四

Formatted: Font: (Default) Times New Roman, 小四

Formatted: Font: (Default) Times New Roman, 小四

Formatted: Font: (Default) Times New Roman, 小四

Formatted: Font: (Default) Times New Roman, 小四

Formatted: Font: (Default) Times New Roman, 小四

Formatted: Font: (Default) Times New Roman, 小四

Formatted: Font: (Default) Times New Roman, 小四

Formatted: Font: (Default) Times New Roman, 小四

Formatted: Font: (Default) Times New Roman, 小四

Formatted: Font: (Default) Times New Roman, 小四

Formatted: Font: (Default) Times New Roman, 小四

Formatted: Font: (Default) Times New Roman, 小四

Formatted: Font: (Default) Times New Roman, 小四

Formatted: Font: (Default) Times New Roman, 小四

models and observations can reach negative values (Figure S12). M3 and M4 tend to overestimate ozone concentrations, M2 slightly overestimates it, and M1, M5, and M7 slightly underestimate it (MBE in Table 4). According to the calculated RMSE in Table 4, M1 and M7 shows relatively better performance in modeling ozone variations. Although WRF-Chem and NU-WRF models were applied at three institutions, different gas phase chemistry schemes were used, which leads to these diversities among predicted ozone concentrations. The impacts of gas phase chemical mechanisms on ozone simulations have been investigated in Knote et al. (2015). The overestimations of ozone concentrations from M3 and M4 primarily occur during nighttime, implying the underestimated titration of ozone by NO_x. Forkel et al. (2015) reported that the RADM2 solver in WRF-Chem has the problem of underestimating ozone titration in areas with high NO emissions, which is the version that applied in M3 and M4.

Formatted: Subscript

Figure 6 shows the comparisons between modeled and observed ground level daily averaged concentrations of SO₂, NO_x, O₃ and PM₁₀ during January 2010 at the Rishiri site in Japan from EANET. The locations of EANET sites are marked in Figure S7. Comparisons at other EANET sites are shown in Figure S15-S18. The models are able to predict the major features in the observations. For example, low values of most pollutants are observed (and predicted) during the first half of the month, followed by elevated values, which peak on January 21. For SO₂, most models show similar capability in producing the temporal variations in observations with slight underestimation (MBE in Table 5). According to the calculated RMSE averaged over all the EANET sites, M2 and the multi-model ensemble mean performed the best. For NO_x, the multi-model ensemble mean shows lower RMSE than any individual model (Table 5). Similar to the comparisons over CARE-China sites, large discrepancies exist in ozone predictions, but the model ensemble mean still shows the lowest RMSE for ozone predictions. PM₁₀ concentrations are largely underestimated by M1 (largest negative MBE: -21.03ug/m³) and overestimated by M5 (highest positive MBE: 3.77ug/m³) (Table 5), which could ~~also~~ be related to the differences in ~~the way sea-salt emissions are treated in the various modelstreatments~~. Spatial distributions of

the monthly near surface concentrations of SO₂, NO_x, O₃ and CO for January 2010 from all participating models are shown in Figure S19. The aerosol spatial distributions are discussed in the following section.

4.3.3 PM_{2.5} and PM_{2.5} chemical composition distribution

Due to different implementations of chemical reactions in the models, predicted PM_{2.5} chemical compositions from participating models differ largely. Figure 7 and Figure 8 show the predicted monthly mean concentrations of sulfate, nitrate, ammonium, BC and OC in PM_{2.5} from all the participating models for January 2010.

M1, M2, M3, M4 and M7 all predict quite low sulfate concentrations in east China, but with considerably enhanced sulfate in southwest~~ern areas of~~ China and west~~ern areas of~~ India. M5 and M6 show similar spatial patterns of sulfate except that M6 produces higher concentrations. The chemical production of sulfate is mainly from gas-phase oxidation of SO₂ by OH radicals and aqueous-phase pathways in cloud water. In cloud water, dissolved SO₂ can be oxidized by O₃, H₂O₂, Fe(III), Mn(II), and NO₂ (Seinfeld and Pandis, 2016). Most chemical transport models have included the above gas phase oxidation of SO₂ by OH₂ and oxidation of dissolved SO₂ by O₃ and H₂O₂ in aqueous phase. Under hazy conditions, radiation is largely reduced due to aerosol dimming effects, and sulfate formation from gas phase and aqueous phase oxidation processes are slowed down, which tend to reduce sulfate concentration. However, field observations exhibit an increase in sulfate concentration during haze episode (Zheng et al., 2015). Cheng et al. (2016) proposed that the reactive nitrogen chemistry in aerosol water could contribute significantly to the sulfate increase due to enhanced sulfate production rates of NO₂ reaction pathway under high

aerosol pH and elevated NO₂ concentrations in the North China Plain (NCP). Wang et al. (2016) also pointed out the aqueous oxidation of SO₂ by NO₂ is key to efficient sulfate formation on fine aerosols with high relative humidity and NH₃ neutralization, or under cloudy conditions. Besides, Zheng et al. (2015) suggested that heterogeneous chemistry on primary aerosols could play an important role in sulfate production and lead to increasing sulfate simulation during haze episodes. X. Huang et al. (2014) found including natural and anthropogenic mineral aerosols can enhance sulfate production through aqueous-phase oxidation of dissolved SO₂ by O₃, NO₂, H₂O₂ and transition metal. Gao et al. (2016b), Wang et al. (2014), and Zhang et al. (2015) also emphasized the importance of multiphase oxidation in winter sulfate production. However, these processes are currently not incorporated in the participating models for this study, which might be responsible for the apparent under-predictions of sulfate concentrations (Figure 9). M5 incorporated heterogeneous chemical reactions on aerosol surface (Li and Han, 2010), which enhances total sulfate production.

M1 and M5 predict relatively small nitrate and ammonium concentrations; while M2, M6 and M7 produce similar magnitudes and spatial patterns of nitrate. Nitrate formation involves both daytime and nighttime chemistry. During daytime, NO₂ can be oxidized by OH to form nitric acid (HNO₃), and by ozone to form NO₃. HNO₃ is easily removed by dry or wet deposition, but NO₃ is easily photolyzed back to NO₂. During nighttime, NO₃ is the major oxidant, which oxidizes NO₂ to form dinitrogen pentoxide (N₂O₅). Homogenous reaction of N₂O₅ with water vapor is possible but very slow while heterogeneous uptake of N₂O₅ onto aerosol particles has been identified as a major sink of N₂O₅ and an important contributor to particulate nitrate (Kim et al., 2014). The MOSAIC aerosol module (Zaveri et al., 2008) coupled with CBMZ gas phase chemistry in WRF-Chem already includes heterogeneous uptake of N₂O₅ since version v3.5.1

646 (Archer-Nicholls et al., 2014), which is the version used by M2, leading to the high production of
647 nitrate. An et al. (2013) incorporated photoexcited nitrogen dioxide molecules, heterogeneous
648 reactions on aerosol surfaces, and direct nitrous acid (HONO) emissions into the WRF-Chem
649 model and found these additional HONO sources ~~can~~ could improve simulations of HONO and
650 nitrate in north China. M7 also predicts high nitrate concentrations (N_2O_5 and NO_2 gases react
651 with liquid water, Zheng et al., 2015), and the predicted lower nitrate concentrations from other
652 models are probably due to missing aqueous phase and heterogeneous chemistry, or the
653 implementations of different gas phase oxidation in these models. Many studies have been
654 conducted regarding sulfate formation issues. Nitrate also account for a large mass fraction in
655 $\text{PM}_{2.5}$ during winter haze events in north China, yet less attention was attracted to fully
656 understand its formation. It is worth furtherly digging into the details about how different
657 processes contribute to high nitrate concentrations in future studies. M3 and M4 do not include
658 the explicit nitrate and ammonium treatment but ammonium is implicitly considered in total
659 $\text{PM}_{2.5}$ mass estimate.

660 The predicted ammonium concentrations are associated with the amounts of sulfate and nitrate,
661 as shown by its similar spatial distribution to sulfate and nitrate. NH_3 neutralizes H_2SO_4 and
662 HNO_3 to form aerosol, so its amount can affect the formation of sulfate, nitrate and ammonium.
663 Since the same emission inventory was used, the amount of ammonia available for neutralizing
664 will not vary greatly among these models. Thus, the rates of H_2SO_4 and HNO_3 production
665 determines the amounts of ammonium. For example, the produced ammonium concentrations are
666 small in M1, similar to ~~their~~ its predicted sulfate and nitrate ~~productions~~ concentrations. High
667 ammonium concentrations are predicted from M6, due to high productions of nitrate and sulfate
668 (Figure 7).

669 The spatial distributions and magnitudes of predicted BC from all participating models are
 670 similar to each other as BC is a primary pollutant ~~whose mass as BC is~~and not impacted by
 671 chemical reactions. The concentrations of BC in the atmosphere are mainly influenced by PBL
 672 mixing and diffusion, aging, deposition (dry deposition and wet scavenging) and advection
 673 processes. Predicted BC concentrations from M2 and M7 are higher than those from other
 674 models, which might be caused by the treatment of aging and deposition (dry deposition and wet
 675 scavenging) processes. For example, in the GOCART aerosol model (M3 and M4), 80% of BC
 676 are assumed to be hydrophobic and then undergo aging to become hydrophilic in an e-folding
 677 time of 1.2 days. Hydrophilic aerosols will go through wet deposition. But in other models like
 678 M2 and M7, BC is assumed to be hydrophobic and, thus ~~the less~~ wet removal ~~is less~~.
 679 The disparity among predicted OC concentrations is mainly associated with the different
 680 treatments of SOA production, given the POC prediction is generally consistent among models
 681 using the same emission inventory. The predicted OC concentrations from M1, M2, and M7 are
 682 close to each other. M1 uses SORGAM (Secondary Organic Aerosol Model) to simulate SOA, but
 683 M2 and M6 did not include any SOA formation mechanism. The similar magnitudes of OC from
 684 M1 suggests that SORGAM in M1 does not produce appreciable amounts of SOA, which is
 685 consistent with the findings in Gao et al. (2016a). Although SOA formation ~~is was~~ implemented
 686 in M5, the production is relatively weak compared to M3 and M4. In the atmosphere, SOA is
 687 mainly formed from the condensation of semi-volatile VOCs, which are the products of ~~from the~~
 688 oxidation of primary VOCs. An empirical 2-product model (Odum et al., 1996) is often used to
 689 simulate SOA formation, but this method was reported to significantly underestimate measured
 690 SOA mass concentrations (Heald et al., 2008). Later, the volatility basis-set (VBS) approach
 691 (Donahue et al., 2006) was developed to represent ~~more realistically~~ the wide range of volatility

of organic compounds and ~~more~~-complex processes~~-. I~~ and it was found that the VBS approach
was able to increase SOA production, and able to reduce observation-simulation biases in many
regions with high emissions (Tsimpidi et al., 2010) including east China (Han et al., 2016). It was
also suggested that primary organic aerosols (POA) are semi-volatile and can evaporate to become
SOA precursors~~-, which promotes the understanding and improvements of SOA modeling~~
(Kanakidou et al., 2005). In M5, the SOA production is calculated using a bulk yield method (~~via~~
Lack et al., (2004), ~~in which~~which ~~the amount of SOA able to be produced from a unit of reacted~~
~~VOC from anthropogenic and biogenic origins are used to represent SOA yields~~uses yields that
represent the maximum amount of SOA able to be produced from a unit of reacted VOCs. However,
the SOA concentration is highly dependent on the yields data. During haze episodes,
photochemistry is reduced due to the aerosol dimming effect, thus aqueous reaction processes on
aerosol water and cloud/fog water could become much more important in producing SOA. R.
Huang et al. (2014) also suggested that low temperature does not significantly reduce SOA
formation rates of biomass burning emissions.

However, m~~M~~ost models over-simplified SOA formation.

In M3 and M4, SOA ~~is~~was treated by assuming that 10% of VOCs from terrestrial source are
converted to OC (Chin et al., 2002), and these models produced high OC concentrations, with a
major contribution from SOA. The 10% yield rate could be unrealistically high during hazy days
because solar radiation was much reduced. Zhao et al. (2015) comprehensively assessed the effect
of organic aerosol aging and intermediate-volatile emissions on OA formation and confirmed their
significant roles. All these results suggest more complicated SOA scheme are needed to improve
organic aerosol simulations during haze events.

714 The different predictions of $PM_{2.5}$ chemical components lead to differences in $PM_{2.5}$ and PM_{10}
 715 concentrations for January 2010, which are shown in the last row of Figure 8. Although spatial
 716 distributions of $PM_{2.5}$ from these models are similar, the underlying causes are different. M2, M3
 717 and M5 simulated higher $PM_{2.5}$ levels in deserts of west China, which are contributed by wind-
 718 blown dust. M1 and M7 failed to produce high $PM_{2.5}$ concentrations in the deserts of west China,
 719 due to omission of dust emissions. ~~M4 presented results in a smaller domain excluding west~~
 720 ~~China. The spatial distributions of predicted wind-blown dust from M5 are slightly different~~
 721 ~~from M2 and M3, with lower concentrations over the Gobi desert (in west Inner Mongolia) (PM_{10}~~
 722 ~~in Figure 8). M2 and M3 used similar GOCART dust emission schemes based on wind speeds~~
 723 ~~and erodible areas, while M5 furtherly considered the dust reduction by vegetation cover, which~~
 724 ~~could partially explain the relatively lower wind-blown dust predictions from M5.~~ The enhanced
 725 $PM_{2.5}$ concentrations in Central China from M2 and M7 are caused by large nitrate production,
 726 as shown in Figure 7.

727 The differences in the predictions of aerosols composition discussed above can be seen clearly in
 728 the comparisons at the Beijing site ~~on during the~~ 13-23 January ~~period~~ when a haze event
 729 occurred in the NCP (Figure 9). ~~Also shown are the observed values.~~ Most models failed to
 730 produce the observed high sulfate concentrations. Only the sulfate predictions from M5 are close
 731 to the observed high values. ~~Sulfate is much lower than observed for all other models, except M6~~
 732 ~~which is too high.~~ M2 and M7 predict reasonable nitrate concentrations. M3 and M4 overpredict
 733 OC during the haze period, but other models underpredict OC concentrations.

734 Figure 10 and 11 show the ensemble mean monthly averaged near-surface $PM_{2.5}$, $PM_{2.5}$
 735 composition, along with the spatial distribution of the coefficient of variation. The coefficient of
 736 variation (CV) is defined as the standard deviation divided by the average (Carmichael et al.,

Formatted: Subscript

2008b), and larger values indicate lower consistency among models. ~~The m~~Mean concentrations of PM_{2.5} and ~~the mean concentrations of~~ PM_{2.5} chemical compositions are high in Sichuan Basin and east China. High ~~coefficient of variation~~CV values are shown in North China for sulfate, and in most areas for nitrate and OC. The diversity in predictions of these species ~~are-is~~ caused by complexity of secondary formation and different ~~model~~ treatments ~~in models as, which have been~~ discussed ~~earlier~~above. Higher consistency is shown for model BC with ~~coefficient of variations~~CV values less than 0.3 in most areas (Figure 10(h)). ~~Coefficient of variations~~The CV values for PM_{2.5} are also low in ~~the~~ North China region, which is consistent with ~~the~~ good performance of PM_{2.5} predictions shown in above comparisons. However, the ~~coefficient of variation~~CV values can reach above 1.6 in northwestern ~~China~~ regions, partially due to discrepancies in dust predictions.

4.3.4 Evaluation of AOD

~~AOD is an indication of aerosol pollution, which tells us how much sunlight is blocked from reaching the surface by suspended aerosols.~~ We used the ~~measurements of~~AOD ~~measurements from at the~~ AERONET and CARE-China ~~sites-networks~~ to evaluate how participating models perform in simulating AOD. The submitted AOD ~~data~~ from all models except M6 ~~are-were~~ at 550nm, and AOD ~~predictions~~ from M6 ~~are-were~~ at 495nm. We used ~~the~~ Angstrom exponent relation (Schuster et al., 2006) to convert AOD ~~from M6~~ at 495nm to 550nm, and all ~~the~~ used AERONET and CARE-China AOD data to 550nm. The locations of ~~the~~ AERONET and CARE-China AOD measurement sites are ~~shown-marked~~ in Figure ~~S5S6~~. Daytime mean AOD are calculated in pairwise manner and the comparisons and performance statistics are shown in Figure 12, 13, and Table 6. On some days, data are missing because AOD cannot be retrieved under serious pollution and cloudy conditions (Gao et al., 2016a). On days with data, the

760 variations of AOD are captured well by all models. However, large disparities exist among
 761 models in the simulated peak AOD values (factor of 2) ~~at monitoring stations~~ during the severe
 762 haze episode ~~on of~~ 15-20 January 2010 (Figure 12 and Figure 13). ~~The participating models~~
 763 ~~exhibit various skill in simulating AOD temporal variation at different sites.~~
 764 ~~At CARE China sites, M7 produces the best correlation coefficient R (0.83) among models at~~
 765 ~~Baoding and Beijing forest sites, M2 produces the highest R (0.86) at Cangzhou site, whereas~~
 766 ~~M5 shows the highest R (0.93) at the Beijing city site. At AERONET sites, M7 shows the~~
 767 ~~highest R (0.81) at Beijing, whereas M2 and M5 produce R as high as 0.91 at Xianghe site,~~
 768 ~~which is about 60km southeast of downtown Beijing. In terms of AOD magnitude, it is~~
 769 ~~interesting to note that during the severest haze days around 19 January 2010, M2 consistently~~
 770 ~~simulates simulated~~ the highest AOD values among models, followed by M5 and M7~~-, while~~
 771 M6 ~~simulates simulated~~ the lowest, ~~and other models in the middle at the sites (Baoding, Beijing~~
 772 ~~City, Beijing Forest, Cangzhou, Beijing, Xianghe) in the north China plain (NCP).~~
 773 In M1, M5, and M7, particle size distribution is described by a lognormal function with a geometric
 774 mean radius and a geometric standard deviation ~~basically~~ based on the OPAC (Optical properties
 775 of aerosols and clouds) database (Hess et al. 1998). In M3 and M4, sulfate, BC and OC are
 776 parameterized in bulk mode, and a sectional scheme is used for sea-salt and dust aerosols. M2 uses
 777 an 8 bins sectional aerosol scheme with size sections ranging from 39nm to 10 μ m. The refractive
 778 index of ~~various different~~ aerosol components in the models are mainly taken from the d'Almeida
 779 et al. (1991) literature or the OPAC database. All models except M6 use a kappa (κ)
 780 parameterization to describe aerosol hygroscopic growth (Petters and Kreidenweis, 2007), in
 781 which ~~the aerosol~~the hygroscopicity κ values largely ~~varies vary~~ among different aerosol chemical

components. ~~For example, such as $\kappa=0$ for black carbon, and $\kappa>0.6$ for inorganic aerosols, but the~~
~~prescribed κ values could be different in the above models.~~ M6 uses a different hygroscopic growth
scheme following Kiehl and Briegleb (1993). WRF-Chem models assume internally mixing
among aerosols within each mode (or size bin) and externally mixing between modes (or size bins),
M5 assumes that inorganic and carbonaceous aerosols are internally mixed ~~and but~~ externally
mixed with soil dust and sea-salt. M6 uses an external mixture assumption among aerosols except
for hydrophilic BC, which is internally mixed with other aerosols in a core-shell way.

~~We first look at the mass concentrations of different aerosol components because of their important~~
~~roles in determining optical properties. As shown in Figure 9, the observed total inorganic aerosol~~
concentration in Beijing on 19 January 2010 ~~is was~~ about $130\mu\text{g}/\text{m}^3$, ~~with sulfate and nitrate being~~
~~about 50 and $65\mu\text{g}/\text{m}^3$, respectively (Figure 9) with sulfate concentrations higher than $50\mu\text{g}/\text{m}^3$ and~~
~~nitrate concentrations over $60\mu\text{g}/\text{m}^3$. However, all~~ The models ~~generally predict a much except M5~~
~~largely underestimated lower~~ sulfate concentrations ~~except that the prediction from M5, which is~~
~~close to observations, and M6, which shows an overprediction.~~ Most models ~~except M2~~
~~underpredicted lower~~ nitrate concentration, ~~in contrast to the overprediction by M2s. In terms of~~
~~inorganic aerosols, which have a similar optical properties, the total concentration (~~ The predicted
~~concentrations of inorganic aerosols~~ (the sum of sulfate, nitrate and ammonium) from M2
($175\mu\text{g}/\text{m}^3$) is higher than observations ~~and other models (Figure 9), and this can explain which~~
~~can partially explain the the~~ largest simulated AOD by M2. ~~The largest simulated AOD by M2~~
~~could also be related to different vertical distributions of aerosols.~~ M6 ~~simulates simulated~~ a similar
level of inorganic aerosols ~~to as~~ M2, but the simulated AOD is lower than other models, which
could be ~~due to~~ caused by a weaker hygroscopicity from a different scheme (Kiehl and Briegleb,
1993) and/or lower simulated RH (see Figure S20). ~~For example, high RH on January 19 are~~

captured by M2 and M6, but underpredicted by M6 (Figure S14a). Although M3 and M4 largely overpredict OC concentrations, ~~their simulated AOD are lower than M1 and M5 because their simulated but~~ inorganic aerosol concentrations are much lower and the mass extinction coefficient of OC ~~has a~~ smaller (mass) extinction coefficient than inorganic aerosols. M1 predicts about three times larger BC concentrations than the observations, ~~although~~ Although the mass extinction coefficient of BC is ~~even~~ larger than inorganic aerosols, the mass concentrations and hygroscopicity of BC are much smaller and weaker than those of inorganic aerosols, leading to relatively lower AOD from M1 simulation. M5 and M7 show high consistency in the simulated AOD due to predict a similar levels of predicted inorganic aerosol concentrations (80~90 $\mu\text{g}/\text{m}^3$) and ~~use a similar hygroscopic growth scheme assumptions, and this can help explain their consistency in the simulated AOD magnitude.~~

As listed in Table 1, ~~only M6 uses external mixing for aerosols, and~~ internal mixing is assumed by ~~other all the participating models except M6~~ for major aerosol compositions. Curci et al. (2015) discussed the impacts of mixing state on simulated AOD and found that external mixing state assumption significantly increase simulated AOD. M6 ~~uses~~ external mixing but shows a relatively lower AOD ~~mainly due to its ignorance of other aerosol species such as dust, sea-salt, etc. because of ignorance of other aerosol species like dust, sea-salt, etc.~~ In general, ~~it appears~~ the magnitudes of simulated inorganic aerosol concentrations and the hygroscopic growth efficiency (affected by varied RH) can ~~account for or~~ explain the simulated variations and magnitudes of AOD in Beijing during the severe haze event, given that most models use the aerosol size lognormal treatments size distributions and internal mixing state are alike among model assumptions.

Table 6 shows the statistics for AOD simulations at ~~NCP~~ the North China sites and at all sites. In the NCP region, R ranges from 0.36~0.74 for all the models. ~~M2, M5 and M7 produce R around 0.7, indicating a better simulation of AOD variations. M2 and M7 exhibit the best R (0.65) for all sites.~~ It is noteworthy that R values at the sites in NCP are larger than ~~that~~ those at all sites, indicating the larger reliability of model inputs (~~emissions and boundary conditions~~) and meteorological simulations in North China. In terms of magnitudes, all models tend to underpredict AOD ~~in the whole domain~~, with NMB of -2.7% to -71% in the NCP, and larger biases (NMB of -21% ~~to~~ -75%) at all sites. ~~M7 shows the smallest MBE (-0.05) and NMB (-2.7%) and M2 produces the smallest RMSE.~~ It is interesting to note that ~~the simulated AOD from the WRF-Chem models differed largely (-12 to -71%) between M1 and M3 at the NCP sites, and the WRF-Chem model using finer grid size (M4) can produced slightly smaller NMB compared with the same model using larger grid size (M3). However, as grid size becomes finer, R and RMSE from M4 may become worse, although AOD magnitude improved.~~ The effect of grid resolution will be a topic of a future paper.

5.4 Summary

The MICS-Asia Phase III Topic 3 examines how current online coupled air quality models perform in reproducing extreme aerosol pollution episodes in North China, and how high aerosol loadings during these episodes interact with radiation and weather. A new anthropogenic emission inventory was developed for this phase (Li et al., 2017), and this inventory along with biogenic, biomass burning, air and ship, and volcano and dust emissions were used ~~provided to all the modeling groups. All modelling groups were required to submit results based on the analysis methodology that documented in this paper.~~ ~~Predicted meteorological variables and air~~

~~pollutants from these modeling groups were compared against each other, and measurements as well. A new anthropogenic emission inventory was developed for this phase (Li et al., 2017), and this inventory along with biogenic, biomass burning, air and ship, and volcano emissions were provided to all modeling groups. All modelling groups were required to submit results based on the analysis methodology that documented in this paper.~~

This paper focused on the evaluation of the predictions of meteorological parameters and the predictions of aerosol mass, composition and optical depth. These factors play important roles in feedbacks impacting weather and climate through radiative and microphysical processes.

Comparisons against daily meteorological variables demonstrated that all models ~~can~~ could capture the observed near surface temperature and water vapor mixing ratio, but near surface wind speeds were overestimated by all models to varying degrees. The observed daily maximum downward shortwave radiation, particularly low values during haze days, were represented in the participating models. Comparisons with measurements of air pollutants, including SO₂, NO_x, CO, O₃, PM_{2.5}, and PM₁₀, from the CARE-China and EANET networks showed that the main features of accumulations of air pollutants are generally represented in the current generation of online coupled air quality models. The observed variations in ~~observed~~-AOD from both the CARE-China and AERONET networks were also reproduced well by the participating models. Differences were found between simulated air pollutants, particularly ozone. While winter time ozone levels are typically low (below 40 ppb) as photochemical pathways are slow, the models captured the synoptic variability but differed in the absolute magnitudes of near surface concentrations. ~~The role of dry deposition and the boundary conditions play important roles.~~

Large differences in the models were found in the predicted PM_{2.5} chemical compositions, especially secondary inorganics and organic carbon. During winter haze events, the production

872 from gas phase chemistry is inhibited, and whether including other aerosol formation pathways
873 (such as aqueous phase chemistry), ~~or how the chemistry is parametrized~~ leads to the large
874 differences between simulated concentrations of secondary inorganic aerosols. In addition,
875 ~~differences in treatments of SOA~~ different SOA treatments also lead to large discrepancies
876 between simulated OC concentrations. Differences in the simulated variations and magnitudes of
877 AOD in Beijing during the ~~severe January 2010~~ haze ~~event~~ episodes could be explained by the
878 differences in simulated inorganic aerosol concentrations and the hygroscopic growth efficiency
879 (affected by varied RH).

880 Results ~~of from~~ this inter-comparison ~~show~~ demonstrate that there remain important issues with
881 current coupled models in predicting winter haze episodes. Low wind speeds play an important
882 role in haze episodes. Current models can predict the low wind speed - high haze relationship,
883 but overestimate the low wind speeds. This contributed to the underestimation of PM_{2.5}. The
884 models also underestimate the production of secondary inorganic aerosols. There is currently a
885 great deal of research focused on inorganic aerosol production under winter haze conditions and
886 new pathways need to be included in the models to improve prediction skills. Furthermore,
887 current models have various treatments of SOA production, ~~and these leading to~~ large wide
888 differences in ~~the contribution of SOA~~ predictions during ~~to~~ winter haze episodes.

889 However, it was also found that using the ensemble mean of the models produced the best
890 prediction skill. While this has been shown for other conditions (for example prediction of high
891 ozone events in the US (McKeen et al., 2004), this is to our knowledge the first time it has been
892 shown for heavy haze events. The uncertainties in predictions ~~in of aerosols mass and~~
893 composition concentrations and optical depth will impact estimates of the aerosol direct and
894 indirect effects during haze events (Gao et al., 2017a, 2017b, 2017c). The results of the MICS-

895 Asia Topic 3 experiments looking at the direct and indirect effects during these heavy haze
896 events ~~is~~are the subjects of companion papers.

898 ACKNOWLEDGMENTS

899 The authors would like to acknowledge support of this project from the National Natural Science
900 Foundation of China (91644217 and NSFC (41620104008)), and ground measurements from
901 Yuesi Wang's research group. The ground observation was supported by the National Natural
902 Science Foundation of China (41222033; 41375036) and the CAS Strategic Priority Research
903 Program Grant (XDA05100102, XDB05020103).

910 Reference

911 Ackermann, I.J., Hass, H., Memmesheimer, M., Ebel, A., Binkowski, F.S. and Shankar, U.M.A.,
912 1998. Modal aerosol dynamics model for Europe: Development and first
913 applications. Atmospheric environment, 32(17), pp.2981-2999.

Formatted: Font: (Default) Times New Roman, 小四, Font color: Auto, Pattern: Clear

Formatted: Indent: Left: 0 cm, Hanging: 2 ch

914 Akimoto, H. (2003). "Global Air Quality and Pollution." *Science*, 302 (5651), 1716-1719.

915 An, J., Li, Y., Chen, Y., Li, J., Qu, Y. and Tang, Y., 2013. Enhancements of major aerosol
916 components due to additional HONO sources in the North China Plain and implications for
917 visibility and haze. *Advances in Atmospheric Sciences*, 30(1), p.57.

918 Anthes, R. A., A cumulus parameterization scheme utilizing a one-dimensional cloud model,
919 *Mon. Wea. Rev.*, 105, 270–286, 1977.

920 Archer-Nicholls, S., et al. (2014). "Gaseous chemistry and aerosol mechanism developments for
921 version 3.5.1 of the online regional model, WRF-Chem." *Geoscientific Model
922 Development*7(6): 2557-2579.

923 Baklanov, A., et al. (2014). "Online coupled regional meteorology chemistry models in Europe:
924 current status and prospects." *Atmospheric Chemistry and Physics*14(1): 317-398.

925 Baklanov, A., Brunner, D., Carmichael, G., Flemming, J., Freitas, S., Gauss, M., Hov, Ø.,
926 Mathur, R., Schlünzen, K.H., Seigneur, C. and Vogel, B., 2017. Key issues for seamless
927 integrated chemistry-meteorology modeling. *Bulletin of the American Meteorological
928 Society*, (2017).

929 Bey, I., et al. (2001). "Global modeling of tropospheric chemistry with assimilated meteorology:
930 Model description and evaluation." *Journal of Geophysical Research:*
931 *Atmospheres*106(D19): 23073-23095.

932 Carlton, A.G., Bhawe, P.V., Napelenok, S.L., Edney, E.O., Sarwar, G., Pinder, R.W., Pouliot,
933 G.A. and Houyoux, M., 2010. Model representation of secondary organic aerosol in
934 CMAQv4. 7. *Environmental science & technology*, 44(22), pp.8553-8560.

935 Carmichael, G. P., L.R. (1984). "An Eulerian transport/transformation/removal model for SO₂
936 and sulfate-I. model development." *Atmospheric Environment*18(5): 937-951.

937 Carmichael, G. P., L.R.; Kitada, T. (1986). "A second generation model for regional-scale
938 transport/chemistry/deposition." *Atmospheric Environment*20(1): 173-188.

Formatted: Font: (Default) Times New Roman, 小四, Font color: Auto, Pattern: Clear

Formatted: Indent: Left: 0 cm, Hanging: 2 ch

939 Carmichael, G. R., Peters, L.R.; Saylor, R. D. (1991). "The STEM-II regional scale acid
940 deposition and photochemical oxidant model-I. an overview of model development and
941 applications." *Atmospheric Environment*25A(10): 2077-2090.

942 Carmichael, G. R., et al. (1998). "Tropospheric ozone production and transport in the springtime
943 in east Asia." *Journal of Geophysical Research: Atmospheres*103(D9): 10649-10671.

944 Carmichael, G. R. C., G.; Hayami, H.; Uno, I.; Cho, S.Y.; Engardt, M.; Kim, S.B.; Ichikawa, Y.;
945 Ikeda, Y.; Woo, J.H.; Ueda, H.; Amann, M. (2002). "The MICS-Asia study: model
946 intercomparison of long-range transport and sulfur deposition in East Asia." *Atmospheric
947 Environment*36: 175-199.

948 Carmichael, G. R., et al. (2008a). "Predicting air quality: Improvements through advanced
949 methods to integrate models and measurements." *Journal of Computational Physics*227(7):
950 3540-3571.

951 Carmichael, G., et al. (2008b). "MICS-Asia II: The model intercomparison study for Asia Phase
952 II methodology and overview of findings." *Atmospheric Environment*42(15): 3468-3490.

953 Carter, W.P., 2000a. Documentation of the SAPRC-99 chemical mechanism for VOC reactivity
954 assessment. Contract, 92(329), pp.95-308.

955 Carter, W.P., 2000b. Implementation of the SAPRC-99 chemical mechanism into the models-3
956 framework. Report to the United States Environmental Protection Agency, January, 29.

957 Cheng, Y. F., Z., G.; Wei, C.; Mu, Q.; Zheng, B.; Wang, Z.; Gao, M.; Zhang, Q.; He, K.;
958 Carmichael, G.; Poschl, U.; Su, Hang (2016). "Reactive nitrogen chemistry in aerosol water
959 as a source of sulfate during haze events in China." *Science Advances* 2(e1601530)

960 Chin, M. G., P.; Kinne, S.; Torres, O.; Holben, B.N.; Duncan, B.N.; Martin, R.V.; Logan, J.A.;
961 Higurashi, A.; Nakajima, T. (2002). "Tropospheric aerosol optical thickness from the
962 GOCART Model and Comparisons with satellite and sun photometer measurements."
963 *Journal of Atmospheric Sciences*(59).

964 [Chou, M.D. and Suarez, M.J., 1994. An efficient thermal infrared radiation parameterization for](#)
 965 [use in general circulation models \(p. 85\). National Aeronautics and Space Administration,](#)
 966 [Goddard Space Flight Center.](#)

967 Curci, G., Hogrefe, C., Bianconi, R., Im, U., Balzarini, A., Baró, R., Brunner, D., Forkel, R.,
 968 Giordano, L., Hirtl, M. and Honzak, L., 2015. Uncertainties of simulated aerosol optical
 969 properties induced by assumptions on aerosol physical and chemical properties: An
 970 AQMEII-2 perspective. *Atmospheric Environment*, 115, pp.541-552.

971 Donahue, N.M., Robinson, A.L., Stanier, C.O. and Pandis, S.N., 2006. Coupled partitioning,
 972 dilution, and chemical aging of semivolatile organics. *Environmental Science &*
 973 *Technology*, 40(8), pp.2635-2643.

974 D’Almeida, G. A., P. Koepke, and E. P. Shettle (1991), *Atmospheric Aero-sols: Global*
 975 *Climatology and Radiative Characteristics*, A. Deepak, Hampton, Va.

976 [Ek, M.B., Mitchell, K.E., Lin, Y., Rogers, E., Grunmann, P., Koren, V., Gayno, G. and Tarpley,](#)
 977 [J.D., 2003. Implementation of Noah land surface model advances in the National Centers](#)
 978 [for Environmental Prediction operational mesoscale Eta model. *Journal of Geophysical*](#)
 979 [Research: Atmospheres, 108\(D22\).](#)

980 ———

981 Emery, C. T., E.; Yarwood, G. (2001). Enhanced meteorological modeling and performance
 982 evaluation for two Texas ozone episodes.

983 Emmons, L. K. W., S.; Hess, P.G.; Lamarque, J-F.; Pfister G.G.; Fillmore, D.; Granier, C.;
 984 Guenther, A.; Kinnison, D.; Laeple, T.; Orlando, J.; Tie, X.; Tyndall, G.; Wiedinmyer, C.;
 985 Baughcum, S.L.; Kloster, S. (2010). "Description and evaluation of the Model for Ozone
 986 and Related chemical Tracers, version 4 (MOZART-4)." *Geoscientific Model*
 987 *Development*3: 43-67.

988 Fast, J.D., Gustafson, W.I., Easter, R.C., Zaveri, R.A., Barnard, J.C., Chapman, E.G., Grell, G.A.
 989 and Peckham, S.E., 2006. Evolution of ozone, particulates, and aerosol direct radiative

990 forcing in the vicinity of Houston using a fully coupled meteorology - chemistry - aerosol
 991 model. *Journal of Geophysical Research: Atmospheres*, 111(D21).

992 Forkel, R., Balzarini, A., Baró, R., Bianconi, R., Curci, G., Jiménez-Guerrero, P., Hirtl, M.,
 993 Honzak, L., Lorenz, C., Im, U. and Pérez, J.L., 2015. Analysis of the WRF-Chem
 994 contributions to AQMEII phase2 with respect to aerosol radiative feedbacks on
 995 meteorology and pollutant distributions. *Atmospheric Environment*, 115, pp.630-645.

996 Galmarini, S., Koffi, B., Solazzo, E., Keating, T., Hogrefe, C., Schulz, M., Benedictow, A.,
 997 Griesfeller, J.J., Janssens-Maenhout, G., Carmichael, G. and Fu, J., 2017. Coordination and
 998 harmonization of the multi-scale, multi-model activities HTAP2, AQMEII3, and MICS-
 999 Asia3: simulations, emission inventories, boundary conditions, and model output
 1000 formats. *Atmospheric Chemistry and Physics*, 17(2), pp.1543-1555.

1001 Ginoux, P., Chin, M., Tegen, I., Prospero, J.M., Holben, B., Dubovik, O. and Lin, S.J., 2001.
 1002 Sources and distributions of dust aerosols simulated with the GOCART model. *Journal of*
 1003 *Geophysical Research: Atmospheres*, 106(D17), pp.20255-20273.

1004 Gao, M., et al. (2015). "Health impacts and economic losses assessment of the 2013 severe haze
 1005 event in Beijing area." *Sci Total Environ* 511: 553-561.

1006 Gao, M., et al. (2016a). "Modeling study of the 2010 regional haze event in the North China
 1007 Plain." *Atmospheric Chemistry and Physics* 16(3): 1673-1691.

1008 Gao, M., et al. (2016b). "Improving simulations of sulfate aerosols during winter haze over
 1009 Northern China: the impacts of heterogeneous oxidation by NO₂." *Frontiers of*
 1010 *Environmental Science & Engineering* 10(5).

1011 Gao, M., et al. (2016c). "Response of winter fine particulate matter concentrations to emission
 1012 and meteorology changes in North China." *Atmospheric Chemistry and Physics* 16(18):
 1013 11837-11851.

1014 Gao, M., et al. (2017a). "Chemical and Meteorological Feedbacks in the Formation of Intense
 1015 Haze Events." *Air Pollution in Eastern Asia: An Integrated Perspective*. Springer, Cham.
 1016 437-452.

Formatted: Font: (Default) Times New Roman, 小四, Font color: Auto, Pattern: Clear

Formatted: Indent: Left: 0 cm, Hanging: 2 ch

1017 Gao, M., et al. (2017b). Distinguishing the roles of meteorology, emission control measures,
 1018 regional transport, and co-benefits of reduced aerosol feedbacks in "APEC
 1019 Blue". Atmospheric Environment, 167, 476-486.

1020 Gao, M., et al. (2017c). "Estimates of Health Impacts and Radiative Forcing in Winter Haze in
 1021 eastern China through constraints of surface PM_{2.5} predictions." Environ Sci Technol.

1022 Gery, M. W. W., G.Z.; Killus, J.P.; Dodge, M.C. (1989). "A photochemical kinetics mechanism
 1023 for urban and regional scale computer modeling " Journal of Geophysical Research 94(D10):
 1024 12925-12956.

1025 [Grell, G.A., 1993. Prognostic evaluation of assumptions used by cumulus](#)
 1026 [parameterizations. Monthly Weather Review, 121\(3\), pp.764-787.](#)

1027 Grell, G. A., et al. (2005). "Fully coupled "online" chemistry within the WRF model."
 1028 Atmospheric Environment 39(37): 6957-6975.

1029 Guenther, A. K., T.; Harley, P.; Wiedinmyer, C.; Palmer, P.I.; Geron, C. (2006). "Estimates of
 1030 global terrestrial isoprene emissions using MEGAN (Model of Emissions of Gases and
 1031 Aerosols from Nature)." Atmospheric Chemistry and Physics 6: 3181-3210.

1032 Han, Zhiwei, Hiromasa Ueda, Kazuhide Matsuda, Renjian Zhang, Kimio Arao, Yutaka Kanai,
 1033 Hisashi Hasome, 2004. Model study on particle size segregation and deposition during
 1034 Asian dust events in March 2002, Journal of Geophysical Research, 109, D19205, doi:
 1035 10.1029/2004jd004920.

1036 Han, Zhiwei. (2010). "Direct radiative effect of aerosols over East Asia with a Regional coupled
 1037 Climate/Chemistry model." Meteorologische Zeitschrift, 19(3): 287-298.

1038 Han Zhiwei, Jiawei Li, Xiangao Xia, Renjian Zhang, 2012. Investigation of direct radiative
 1039 effects of aerosols in dust storm season over East Asia with an online
 1040 coupled regional climate-chemistry-aerosol model. Atmospheric Environment, 54, 688-699.

1041 Han Zhiwei, Jiawei Li, Weidong Guo, Zhe Xiong, Wu Zhang, 2013. A study of dust radiative
 1042 feedback on dust cycle and meteorology over East Asia by a coupled regional climate-
 1043 chemistry-aerosol model. Atmospheric Environment, 68, 54-63.

1044 Han Zhiwei et al.,2016. Modeling organic aerosols over east China using a volatility basis-set
 1045 approach with aging mechanism in a regional air quality model. Atmospheric Environment
 1046 124 , 186-198.

1047 Heald, C.L., Henze, D.K., Horowitz, L.W., Feddema, J., Lamarque, J.F., Guenther, A., Hess,
 1048 P.G., Vitt, F., Seinfeld, J.H., Goldstein, A.H. and Fung, I., 2008. Predicted change in global
 1049 secondary organic aerosol concentrations in response to future climate, emissions, and land
 1050 use change. Journal of Geophysical Research: Atmospheres, 113(D5).

1051 Henderson-Sellers, A., 1993. A factorial assessment of the sensitivity of the BATS land-surface
 1052 parameterization scheme. Journal of climate, 6(2), pp.227-247.

1053 Hess, M., Koepke, P., Schuit, I., 1998. Optical properties of aerosols and clouds: the software
 1054 package OPAC. Bull. Am. Meteorol. Soc. 79, 831-844.

1055 He, H., Wang, Y., Ma, Q., Ma, J., Chu, B., Ji, D., Tang, G., Liu, C., Zhang, H. and Hao, J., 2014.
 1056 Mineral dust and NOx promote the conversion of SO₂ to sulfate in heavy pollution
 1057 days. Scientific reports, 4, p.4172.

1058 Holben, B. N., Eck, T.F., Slutsker, I., Tanre, D., Buis, J.P., Setzer, A., Vermote, E., Reagan, J.A.,
 1059 Kaufman, Y.J., Nakajima, T. and Lavenue, F. (1998). "AERONET—A federated instrument
 1060 network and data archive for aerosol characterization." Remote sensing of
 1061 environment66(1): 1-16.

1062 Holloway, T., et al. (2008). "MICS-Asia II: Impact of global emissions on regional air quality in
 1063 Asia." Atmospheric Environment42(15): 3543-3561.

1064 Holtslag, A. A. M., and B. A. Boville, Local versus nonlocal boundary-layer diffusion in a global
 1065 climate model, J. Climate, 6, 1993.

1066 Hong, S.Y. and Pan, H.L., 1996. Nonlocal boundary layer vertical diffusion in a medium-range
 1067 forecast model. Monthly weather review, 124(10), pp.2322-2339.

1068 Huang, M., Carmichael, G.R., Pierce, R.B., Jo, D.S., Park, R.J., Flemming, J., Emmons, L.K.,
 1069 Bowman, K.W., Henze, D.K., Davila, Y. and Sudo, K., 2017. Impact of intercontinental

Formatted: Font: (Default) Times New Roman, 小四, Font color: Auto, Pattern: Clear

Formatted: Indent: Left: 0 cm, Hanging: 2 ch

1070 pollution transport on North American ozone air pollution: an HTAP phase 2 multi-model
 1071 study. *Atmospheric Chemistry and Physics*, 17(9), pp.5721-5750.

1072 Huang, X., Song, Y., Zhao, C., Li, M., Zhu, T., Zhang, Q. and Zhang, X., 2014. Pathways of
 1073 sulfate enhancement by natural and anthropogenic mineral aerosols in China. *Journal of*
 1074 *Geophysical Research: Atmospheres*, 119(24).

1075 Huang, R.J., Zhang, Y., Bozzetti, C., Ho, K.F., Cao, J.J., Han, Y., Daellenbach, K.R., Slowik,
 1076 J.G., Platt, S.M., Canonaco, F. and Zotter, P., 2014. High secondary aerosol contribution to
 1077 particulate pollution during haze events in China. *Nature*, 514(7521), pp.218-222.

1078 Iacono, M.J., Delamere, J.S., Mlawer, E.J., Shephard, M.W., Clough, S.A. and Collins, W.D.,
 1079 2008. Radiative forcing by long-lived greenhouse gases: Calculations with the AER
 1080 radiative transfer models. *Journal of Geophysical Research: Atmospheres*, 113(D13).

1081 Jacobson, M. Z., 2001: Global direct radiative forcing due to multicomponent anthropogenic and
 1082 natural aerosols. *J. Geophys. Res.*, 106, 1551–1568.

1083 Janssens-Maenhout, G., et al. (2015). "HTAP_v2.2: a mosaic of regional and global emission
 1084 grid maps for 2008 and 2010 to study hemispheric transport of air pollution." *Atmospheric*
 1085 *Chemistry and Physics* 15(19): 11411-11432.

1086 Kalnay, E., Kanamitsu, M., Kistler, R., Collins, W., Deaven, D., Gandin, L., Iredell, M., Saha,
 1087 S., White, G., Woollen, J. and Zhu, Y., 1996. The NCEP/NCAR 40-year reanalysis
 1088 project. *Bulletin of the American meteorological Society*, 77(3), pp.437-471.

1089 Kanakidou, M., Seinfeld, J.H., Pandis, S.N., Barnes, I., Dentener, F.J., Facchini, M.C.,
 1090 Dingenen, R.V., Ervens, B., Nenes, A.N.C.J.S.E., Nielsen, C.J. and Swietlicki, E., 2005.
 1091 Organic aerosol and global climate modelling: a review. *Atmospheric Chemistry and*
 1092 *Physics*, 5(4), pp.1053-1123.

1093 Kim, S. W., et al. (2009). "NO₂ columns in the western United States observed from space and
 1094 simulated by a regional chemistry model and their implications for NO_x emissions." *Journal*
 1095 *of Geophysical Research* 114(D11).

Formatted: Font: (Default) Times New Roman, 小四, Font color: Auto, Pattern: Clear

Formatted: Indent: Left: 0 cm, Hanging: 2 ch

1096 Kim, Y. J. S., S.N.; Carmichael, G.R.; Riemer, N.; Stanier, C.O. (2014). "Modeled aerosol
1097 nitrate formation pathways during wintertime in the Great Lakes region of North America."
1098 Journal of Geophysical Research: Atmospheres 119: 12420-12445.

1099 Kiehl, J.T., Briegleb, B.P., 1993. The relative roles of sulfate aerosols and greenhouse gases in
1100 climate forcing. Science 260, 311-314.

1101 Knote, C., et al. (2015). "Influence of the choice of gas-phase mechanism on predictions of key
1102 gaseous pollutants during the AQMEII phase-2 intercomparison." Atmospheric
1103 Environment 115: 553-568.

1104 Lack, D. A., et al. (2004). "Seasonal variability of secondary organic aerosol: A global modeling
1105 study." Journal of Geophysical Research: Atmospheres 109(D3): n/a-n/a.

1106 Lelieveld, J., et al. (2015). "The contribution of outdoor air pollution sources to premature
1107 mortality on a global scale." Nature 525(7569): 367-371.

1108 Li, M., Zhang, Q., Streets, D.G., He, K.B., Cheng, Y.F., Emmons, L.K., Huo, H., Kang, S.C., Lu,
1109 Z., Shao, M. and Su, H., 2014. Mapping Asian anthropogenic emissions of non-methane
1110 volatile organic compounds to multiple chemical mechanisms. Atmospheric Chemistry and
1111 Physics, 14(11), p.5617.

1112 Li, M., et al. (2017). "MIX: a mosaic Asian anthropogenic emission inventory under the
1113 international collaboration framework of the MICS-Asia and HTAP." Atmospheric
1114 Chemistry and Physics 17(2): 935-963.

1115 Li, J. and Han, Z., 2016. Aerosol vertical distribution over east China from RIEMS-Chem
1116 simulation in comparison with CALIPSO measurements. Atmospheric Environment, 143,
1117 pp.177-189.

1118 Lin, Y.L., Farley, R.D. and Orville, H.D., 1983. Bulk parameterization of the snow field in a
1119 cloud model. Journal of Climate and Applied Meteorology, 22(6), pp.1065-1092.

1120 McKeen, S., Wilczak, J., Grell, G., Djalalova, I., Peckham, S., Hsie, E.Y., Gong, W., Bouchet,
1121 V., Menard, S., Moffet, R. and McHenry, J., 2005. Assessment of an ensemble of seven

Formatted: Font: (Default) Times New Roman, 小四, Font color: Auto, Pattern: Clear

Formatted: Indent: Left: 0 cm, Hanging: 2 ch

real - time ozone forecasts over eastern North America during the summer of 2004. Journal of Geophysical Research: Atmospheres, 110(D21).

Maloney, E.D. and Hartmann, D.L., 2001. The sensitivity of intraseasonal variability in the NCAR CCM3 to changes in convective parameterization. Journal of Climate, 14(9), pp.2015-2034.

Makar, P.A., Gong, W., Milbrandt, J., Hogrefe, C., Zhang, Y., Curci, G., Žabkar, R., Im, U., Balzarini, A., Baró, R. and Bianconi, R., 2015a. Feedbacks between air pollution and weather, Part 1: Effects on weather. Atmospheric Environment, (115), pp.442-469.

Makar, P.A., Gong, W., Hogrefe, C., Zhang, Y., Curci, G., Žabkar, R., Milbrandt, J., Im, U., Balzarini, A., Baró, R. and Bianconi, R., 2015b. Feedbacks between air pollution and weather, part 2: effects on chemistry. Atmospheric environment, 115, pp.499-526.

Menon, S. H., J.; Nazarenko, N.; Luo, Y. (2002). "Climate Effects of Black Carbon Aerosols in China and India." Science.

Mlawer, E.J., Taubman, S.J., Brown, P.D., Iacono, M.J. and Clough, S.A., 1997. Radiative transfer for inhomogeneous atmospheres: RRTM, a validated correlated - k model for the longwave. Journal of Geophysical Research: Atmospheres, 102(D14), pp.16663-16682.

Morrison, H., Curry, J.A. and Khvorostyanov, V.I., 2005. A new double-moment microphysics parameterization for application in cloud and climate models. Part I: Description. Journal of the Atmospheric Sciences, 62(6), pp.1665-1677.

Nenes, A., Pandis, S.N. and Pilinis, C., 1998. ISORROPIA: A new thermodynamic equilibrium model for multiphase multicomponent inorganic aerosols. Aquatic geochemistry, 4(1), pp.123-152.

Nogherotto, R., Tompkins, A.M., Giuliani, G., Coppola, E. and Giorgi, F., 2016. Numerical framework and performance of the new multiple-phase cloud microphysics scheme in RegCM4. 5: precipitation, cloud microphysics, and cloud radiative effects. Geoscientific Model Development, 9(7), pp.2533-2547.

1148 Odum, J.R., Huffman, T., Bowman, F., Collins, D., Flagan, R.C., Seinfeld, J.H.,
 1149 1996. Gas/Particle partitioning and secondary organic aerosol yields. Environ. Sci. Technol.
 1150 30, 2580-2585.

1151 Peters-Lidard, C. D., E. M. Kemp, T. Matsui, J.A. Santanello Jr., S.V. Kumar, J.P. Jacob, T.
 1152 Clune, W.-K. Tao, M. Chin, A. Hou, J.L. Case, D. Kim, K.-M. Kim, W. Lau, Y. Liu, J. Shi,
 1153 D. Starr, Q. Tan, Z. Tao, B.F. Zaitchik, B. Zavodsky, S.Q. Zhang, and M. Zupanski,
 1154 Integrated modeling of aerosol, cloud, precipitation and land processes at satellite-resolved
 1155 scales. Environmental Modeling & Software, 67, 149-159,
 1156 doi:10.1016/j.envsoft.2015.01.007, 2015.

1157 Petters, M.D., Kreidenweis, S.M., 2007. A single parameter representation of hygroscopic
 1158 growth and cloud condensation nucleus activity. Atmos. Chem. Phys. 7, 1961-1971.

1159 Ramanathan, V. C., G. (2008). "Global and regional climate changes due to black carbon."
 1160 Nature Geoscience 1(4): 221-227.

1161 Randerson, J.T., G.R. van der Werf, L. Giglio, G.J. Collatz, and P.S. Kasibhatla. 2015. Global
 1162 Fire Emissions Database, Version 4 (GFEDv4). ORNL DAAC, Oak Ridge, Tennessee,
 1163 USA. <http://dx.doi.org/10.3334/ORNLDAAC/1293>

1164 Reisner, J., RaSmuSSen, R.M. and Bruintjes, R.T., 1998. Explicit forecasting of supercooled
 1165 liquid water in winter storms using the MM5 mesoscale model. Quarterly Journal of the
 1166 Royal Meteorological Society, 124(548), pp.1071-1107.

1167 San José, R., Pérez, J.L., Balzarini, A., Baró, R., Curci, G., Forkel, R., Galmarini, S., Grell, G.,
 1168 Hirtl, M., Honzak, L. and Im, U., 2015. Sensitivity of feedback effects in CBMZ/MOSAIC
 1169 chemical mechanism. Atmospheric Environment, 115, pp.646-656.

1170 Schell, B., Ackermann, I.J., Hass, H., Binkowski, F.S. and Ebel, A., 2001. Modeling the
 1171 formation of secondary organic aerosol within a comprehensive air quality model
 1172 system. Journal of Geophysical Research: Atmospheres, 106(D22), pp.28275-28293.

1173 Schuster, G. L., et al. (2006). "Angstrom exponent and bimodal aerosol size distributions."
 1174 Journal of Geophysical Research 111(D7).

Formatted: Font: (Default) Times New Roman, 小四, Font color: Auto, Pattern: Clear

Formatted: Indent: Left: 0 cm, Hanging: 2 ch

Formatted: Font: (Default) Times New Roman, 小四

Formatted: Font: (Default) Times New Roman, 小四, Font color: Auto, Pattern: Clear

Formatted: Indent: Left: 0 cm, Hanging: 2 ch

1175
1176 Seinfeld, J.H. and Pandis, S.N., 2016. Atmospheric chemistry and physics: from air pollution to
1177 climate change. John Wiley & Sons.

1178 Stockwell, W.R., Middleton, P., Chang, J.S. and Tang, X., 1990. The second generation regional
1179 acid deposition model chemical mechanism for regional air quality modeling. Journal of
1180 Geophysical Research: Atmospheres, 95(D10), pp.16343-16367.

1181 Stockwell, W. R., et al. (1997). "A new mechanism for regional atmospheric chemistry
1182 modeling." Journal of Geophysical Research: Atmospheres 102(D22): 25847-25879.

1183 Stoiber, R. E. W., S.N.; Huebert, B. (1987). "Annual contribution of sulfur dioxide to the
1184 atmosphere by volcanoes." Journal of Volcanology and Geothermal Research 33: 1-8.

1185 Streets, D. G., et al. (2003). "Biomass burning in Asia: Annual and seasonal estimates and
1186 atmospheric emissions." Global Biogeochemical Cycles 17(4): n/a-n/a.

1187 Tao, W.K., Simpson, J., Baker, D., Braun, S., Chou, M.D., Ferrier, B., Johnson, D., Khain, A.,
1188 Lang, S., Lynn, B. and Shie, C.L., 2003. Microphysics, radiation and surface processes in
1189 the Goddard Cumulus Ensemble (GCE) model. Meteorology and Atmospheric
1190 Physics, 82(1), pp.97-137.

1191 Tao, Z., J. A. Santanello, M. Chin, S. Zhou, Q. Tan, E. M. Kemp, and C. D. Peters-Lidard, Effect
1192 of land cover on atmospheric processes and air quality over the continental United States –
1193 A NASA Unified WRF (NU-WRF) model study. Atmospheric Chemistry & Physics, 13:
1194 6207-6226, doi: 10.5194/acp-13-6207-2013, 2013.

1195 Tao, Z., H. Yu, and M. Chin, Impact of transpacific aerosol on air quality over the United States:
1196 A perspective from aerosol-cloud-radiation interactions. Atmospheric Environment, 125:
1197 48-60, doi:10.1016/j.atmosenv.2015.10.083, 2016.

1198 Tao, Z., H. Yu, and M. Chin, The role of aerosol-cloud-radiation interactions in regional air
1199 quality – A NU-WRF study over the United States. Atmosphere, 6, 1045-1068,
1200 doi:10.3390/atmos6081045, 2015.

Formatted: Indent: Left: 0 cm, First line: 0 ch

Formatted: Font: (Default) Times New Roman, 小四, Font color: Auto, Pattern: Clear

Formatted: Indent: Left: 0 cm, Hanging: 2 ch

1201 Tsimpidi et al., 2010. Evaluation of the volatility basis-set approach for the simulation of organic
 1202 aerosol formation in the Mexico City metropolitan area. *Atmos. Chem. Phys.*, 10, 525–546.
 1203 *Atmospheres*102(D23): 28589-28612.

1204 Yu, S., Mathur, R., Pleim, J., Wong, D., Gilliam, R., Alapaty, K., Zhao, C. and Liu, X., 2013.
 1205 Aerosol indirect effect on the grid-scale clouds in the two-way coupled WRF-CMAQ:
 1206 model description, development, evaluation and regional analysis. *Atmospheric Chemistry*
 1207 *and Physics Discussion*, p.25649.

1208 Wang et al., 2016. Persistent sulfate formation from London Fog to Chinese haze. *PNAS*,
 1209 113(48), 13630–13635.

1210 Wang, J., et al. (2014). "Impact of aerosol–meteorology interactions on fine particle pollution
 1211 during China’s severe haze episode in January 2013." *Environmental Research Letters*9(9):
 1212 094002.

1213 Wang, T., et al. (2010). "Investigations on direct and indirect effect of nitrate on temperature and
 1214 precipitation in China using a regional climate chemistry modeling system." *Journal of*
 1215 *Geophysical Research*115.

1216 Wang, Z. Maeda, T.; Hayashi, M.; Hsiao, L.F.; Liu, K.Y. (2001). "A nested air quality
 1217 prediction modeling system for urban and regional scales: application for high-ozone
 1218 episode in Taiwan." *Water, Air, & Soil Pollution*130(1): 391-396

1219 Xiao, H., et al. (1997). "Long-range transport of Sox and dust in East Asia during the PEM B
 1220 Experiment." *Journal of Geophysical Research*:

1221 Xin, J., et al. (2015). "The Campaign on Atmospheric Aerosol Research Network of China:
 1222 CARE-China." *Bulletin of the American Meteorological Society*96(7): 1137-1155.

1223 Zaveri, R. A., et al. (2008). "Model for Simulating Aerosol Interactions and Chemistry
 1224 (MOSAIC)." *Journal of Geophysical Research*113(D13).

1225 Zaveri, R. A. and L. K. Peters (1999). "A new lumped structure photochemical mechanism for
1226 large-scale applications." Journal of Geophysical Research: Atmospheres 104(D23): 30387-
1227 30415.

1228 Zhao, B., Wang, S., Donahue, N.M., Jathar, S.H., Huang, X., Wu, W., Hao, J. and Robinson,
1229 A.L., 2016. Quantifying the effect of organic aerosol aging and intermediate-volatility
1230 emissions on regional-scale aerosol pollution in China. Scientific reports, 6, p.28815.

1231 Zhang, Y., et al. (2010). "Simulating chemistry–aerosol–cloud–radiation–climate feedbacks over
1232 the continental U.S. using the online-coupled Weather Research Forecasting Model with
1233 chemistry (WRF/Chem)." Atmospheric Environment 44(29): 3568-3582.

1234 Zheng et al., 2015. Heterogeneous chemistry: a mechanism missing in current models to explain
1235 secondary inorganic aerosol formation during the January 2013 haze episode in North
1236 China. Atmos. Chem. Phys., 15, 2031–204

1237

1238
1239
1240
1241
1242
1243
1244
1245
1246
1247
1248

Participating models in Topic 3

Formatted: Font: (Default) Times New Roman, 小四, Font color: Auto, Pattern: Clear
Formatted: Indent: Left: 0 cm, Hanging: 2 ch

Models	M1: WRF-Chem	M2: WRF-Chem	M3: NU-WRF	M4: NU-WRF	M5: RIEMS-Chem	M6: RegCCMS	M7: WRF-CMAQ
Modelling Group	Pusan National University	University of Iowa	USRA/NASA A	USRA/NASA	Institute of Atmospheric Physics	Nanjing University	University of Tennessee
Grid Resolution	45km	50km	45km	15km	60km	50km	45km
Vertical Layers	40 layers to 50mb	27 layers to 50mb	60 layers to 20mb	60 layers to 20mb	16 layers to 100mb	18 layers to 50mb	34 layers to 50mb
Gas phase chemistry	RACM-ESRL	CBMZ	RADM2	RADM2	CBM4	CBM4	SAPRC99
Aerosols	MADE/SOR-GAM; modal scheme	MOSAIC-8bin; sectional scheme	GOCART; bulk scheme	GOCART; bulk scheme	Sulfate, nitrate, ammonium, BC, OC, SOA, 5 bins of soil dust, and 5 bins of sea salt modal scheme; GEOS-Chem	Sulfate, nitrate, ammonium, BC and POC; bulk scheme	AE06 modal scheme
Chemical Boundary Conditions	Climatological data from NALROM	MOZART	MOZART GOCART	MOZART GOCART	GEOS-Chem	Climatological data	GEOS-Chem
Meteorological Boundary Conditions	NCEP FNL	NCEP FNL	NASA MERRA	NASA MERRA	NCEP FNL	NCEP-NCAR	NCEP FNL
BVOC emissions	prescribed	Internal calculation	Internal calculation	Internal calculation	prescribed	NA	Internal calculation
Dust	NA	GOCART AFWA	GOCART dust	GOCART dust	Han et al. (2004)	NA	NA
Microphysics	Lin scheme (Lin et al., 1983)	Morrison double-moment (Morrison et al., 2005)	GCE (Goddard Cumulus Ensemble)	GCE (Tao et al., 2003)	Reisner et al., 1998-mixed phase	Nogherotto et al., (2016)	Lin scheme
Longwave radiation	RRTMG (Iacono et al., 2008)	RRTMG	Goddard (Chou et al., 1994)	Goddard	CCM3 (Maloney et al., 2001)	CCM3	RRTM (Mlawer et al. 1997)
Shortwave radiation	RRTMG	RRTMG	Goddard	Goddard	Revised CCM3	CCM3	Goddard
Boundary Layer	Yonsei University	Yonsei University	YSU	YSU	MRF (Hong and Pan, 1996)	Holtslag et al., (1990)1993}	Yonsei University

Table	Cu physics	Grell 3D (Grell, 1993)	Grell 3D	Grell 3D	Grell 3D	Grell 3D	Anthes et al. (1997, 1977)	Grell 3D
1	Surface physics	Thermal diffusion	Unified Noah (Ek et al., 2003)	Unified Noah	Unified Noah	BATS (Henderson-Sellers, 1993)	BATS BATS	<u>Unified Noah</u>
NA	Aerosol-radiation	Yes	Yes	Yes	Yes	Yes	Yes	Yes ¹
	Aerosol-microphysics	Yes	Yes	Yes	Yes	Yes	Yes	No
	Mixing state	Internal mixing	Internal mixing	Internal mixing	Internal mixing	Internal mixing among inorganic aerosols and BC and OC, and external mixing between dust, sea-salt and other aerosols	External mixing	Internal mixing

represents ~~not available~~ not considered in the simulation; M1: WRF-Chem v3.7.1; M2: WRF-Chem v3.5.1; M3&M4: NU-WRF v7lis7-3.5.1-p3; M5: RIMES-Chem; M6: RegCCMS; M7: WRFv3.4.1&CMAQv5.0.2

1 Online coupled WRF-CMAQ only considers aerosol-radiation interactions but no aerosol indirect effects. The WRF-CMAQ results shown in this paper are from an offline simulation (aerosol-radiation interaction was turned off).

Formatted: Font: Bold

Formatted: Superscript

Table 2 CARE-Chine network sites

ID	Site name	Characteristics	Longitude	Latitude
1	Beijing	<u>Air quality*</u> , AOD	116.37	39.97
2	Tianjin	Air quality*	117.21	39.08
3	Shijiazhuang	Air quality	114.53	38.03
4	Xianghe	Air quality	116.96	39.75
65	Beijing Forest	AOD	115.43	39.97
67	Baoding	AOD	115.51	38.87
87	Cangzhou	AOD	116.80	38.28
89	Shenyang	AOD	123.63	41.52
910	Jiaozhou Bay	AOD	120.18	35.90

*Air quality: surface PM_{2.5}, PM₁₀, SO₂, NO_x, CO, O₃

Table 3 Performance Statistics of Meteorology Variables (RMSE and MBE units: degree for T2; g/kg for Q2; m/s for WS10; W/m² for SWDOWN)

Metrics	Models	T2	Q2	WS10	SWDOWN South	SWDOWN North
RMSE	M1	0.64	0.14	2.04	86.32	69.39
	M2	0.68	0.10	0.95	96.71	72.76
	M3	2.34	0.16	1.16	60.34	59.56
	M4	2.90	0.43	1.44	100.34	74.89
	M5	2.97	0.46	0.91	91.06	65.27
	M6	3.57	0.76	2.48	85.63	222.00
	M7	2.05	0.17	0.22	158.10	218.67
	Ensemble	1.81	0.10	1.28	81.96	62.51
MBE	M1	-0.19	0.02	2.01	66.58	59.94
	M2	-0.60	-0.01	0.91	83.88	62.38
	M3	-2.18	-0.04	1.11	36.44	47.74
	M4	-2.09	0.11	1.40	26.78	33.59
	M5	-2.73	0.43	0.74	49.06	51.00
	M6	-3.06	-0.56	2.37	-0.49	-202.26
	M7	-2.02	-0.12	0.15	145.24	159.02
	Ensemble	-1.71	-0.02	1.25	65.54	36.37

NMB (%)	M1	-0.07%	0.19%	17.58%	14.61%	13.34%
	M2	-0.21%	-0.12%	7.94%	18.41%	13.88%
	M3	-0.79%	-0.34%	9.73%	8.00%	10.63%
	M4	-0.75%	0.95%	12.26%	5.88%	7.48%
	M5	-0.98%	3.65%	6.45%	10.77%	11.35%
	M6	-1.10%	-4.77%	20.73%	-0.11%	-45.02%
	M7	-0.72%	-1.05%	1.31%	31.88%	35.39%
	Ensemble	-0.61%	-0.14%	10.98%	14.38%	8.10%

Table 4 Performance Statistics of Air Pollutants at the CARE-China sites (RMSE and MBE units: ppbv for gases and $\mu\text{g}/\text{m}^3$ for PM)

Metrics	Models	SO₂	NO_x	O₃	PM_{2.5}	PM₁₀		SO₂	NO_x	O₃	PM_{2.5}	PM₁₀
r	M1	0.76	0.60	0.46	0.85	0.76	MBE	-17.14	-5.53	-1.54	55.69	30.70
	M2	0.77	0.65	0.48	0.90	0.85		2.10	33.41	2.53	48.44	12.94
	M3	0.69	0.66	0.39	0.85	0.68		-15.89	-8.00	23.93	8.13	-19.92
	M4	0.67	0.61	0.42	0.88	0.73		-9.98	0.28	24.49	23.12	-3.23
	M5	0.72	0.73	0.39	0.91	0.84		-9.69	64.29	-5.30	1.68	-52.49
	M6	0.62	0.48	-	-	-		-27.53	-29.98	-	-	-
	M7	0.57	0.58	0.48	0.82	0.77		-25.56	7.85	-3.09	43.59	-21.00
	Ensemble	0.79	0.71	0.51	0.94	0.87		-14.81	8.90	6.84	30.11	-8.83
RMSE	M1	27.63	33.51	6.40	73.37	79.06	NMB (%)	-14.05	-5.41	7.37	63.57	18.93
	M2	21.00	66.30	8.15	72.44	80.72		12.13	69.58	39.87	54.07	6.38
	M3	29.50	36.87	24.76	47.20	78.21		-10.44	-6.26	306.33	9.67	-12.41
	M4	26.86	36.10	25.34	49.13	72.25		0.31	4.51	316.99	27.03	-1.78
	M5	32.17	87.48	7.90	45.32	81.00		6.83	127.45	-38.49	0.52	-32.94
	M6	33.95	48.62	-	-	-		-51.28	-48.59	-	-	-
	M7	34.75	35.88	6.89	64.25	70.19		-37.87	18.32	-7.78	48.92	-12.78
	Ensemble	24.10	29.12	8.86	45.25	56.65		-13.48	22.80	104.04	33.96	-5.77

MFB (%)	M1	-17.32	5.26	-5.06	64.34	21.98	MFE (%)	53.73	43.79	54.54	69.92	41.95
	M2	9.09	32.82	19.88	51.18	3.44		43.18	73.39	60.79	59.87	39.35
	M3	-12.96	4.52	113.60	32.67	-4.62		57.87	46.69	113.60	50.10	36.83
	M4	1.53	15.34	114.35	45.27	6.07		46.30	48.13	114.35	55.03	34.72
	M5	-20.24	67.25	-62.65	16.88	-35.15		63.69	72.07	80.92	48.17	45.09
	M6	-77.13	-56.89	-	-	-		84.21	69.66	-	-	-
	M7	-46.67	21.80	-19.50	57.19	-7.02		72.35	49.18	60.64	66.27	35.83
	Ensemble	-14.17	26.41	62.86	50.61	3.12		43.13	42.94	71.14	55.86	28.05

Table 5 Performance Statistics of Air Pollutants at the EANET sites (RMSE and MBE units: ppbv for gases and $\mu\text{g}/\text{m}^3$ for PM)

Metrics	Models	SO₂	NO_x	O₃	PM₁₀		SO₂	NO_x	O₃	PM₁₀
r	M1	0.57	0.64	0.14	0.59		-0.68	0.68	-6.16	-21.03
	M2	0.59	0.45	0.30	0.75		-0.45	-0.39	5.50	3.12
	M3	0.50	0.55	0.26	0.51		-0.37	-0.21	3.67	3.55
	M4	0.45	0.55	0.25	0.49		-0.57	-0.61	4.28	2.96
	M5	0.58	0.54	0.01	0.03		-0.57	1.28	4.67	3.77
	M6	0.33	0.24	-	-	MBE	0.32	-1.68	-	-
	M7	0.53	0.49	0.38	0.55		-0.03	0.64	-1.89	-15.75
	Ensemble	0.60	0.66	0.32	0.59		-0.34	-0.07	1.68	-3.89

NMB (%)	M1	-46.45	41.49	-15.03	-82.29		1.18	1.37	8.23	23.39
	M2	-29.64	-29.75	13.47	18.90		1.01	1.35	7.29	10.01
	M3	-25.42	-17.75	9.01	19.46		1.02	1.02	6.44	13.71
	M4	-39.63	-35.84	10.47	16.95	RMSE	1.14	0.97	6.35	13.78
	M5	-34.23	38.50	11.38	31.80		1.27	2.75	12.27	23.10
	M6	12.63	-93.57	-	-		1.38	1.85	-	-
	M7	17.42	31.47	-4.71	-56.18		1.04	1.57	6.52	18.76
	Ensemble	-20.76	-10.79	4.10	-8.56		0.96	0.79	4.98	11.69

Table 6 Performance Statistics of AOD

Metrics	Models	M1	M2	M3	M4	M5	M6	M7	Ensemble
R	North	0.63	0.74	0.57	0.51	0.68	0.36	0.71	0.77
	China								
	All	0.60	0.65	0.46	0.42	0.53	0.33	0.64	0.75
MBE	North	-0.25	-0.10	-0.09	-0.07	-0.13	-0.21	-0.05	-0.03
	China								
	All	-0.18	-0.02	-0.01	-0.01	-0.01	-0.11	0.00	-0.12
NMB (%)	North	-71.25	-23.28	-12.63	-9.59	-28.34	-59.19	-2.70	-30.17
	China								
	All	-74.94	-30.69	-25.68	-23.64	-28.24	-55.38	-21.12	-28.91
RMSE	North	0.35	0.20	0.26	0.28	0.24	0.36	0.22	0.22
	China								
	All	1.16	1.13	1.15	1.15	1.15	1.17	1.14	0.20

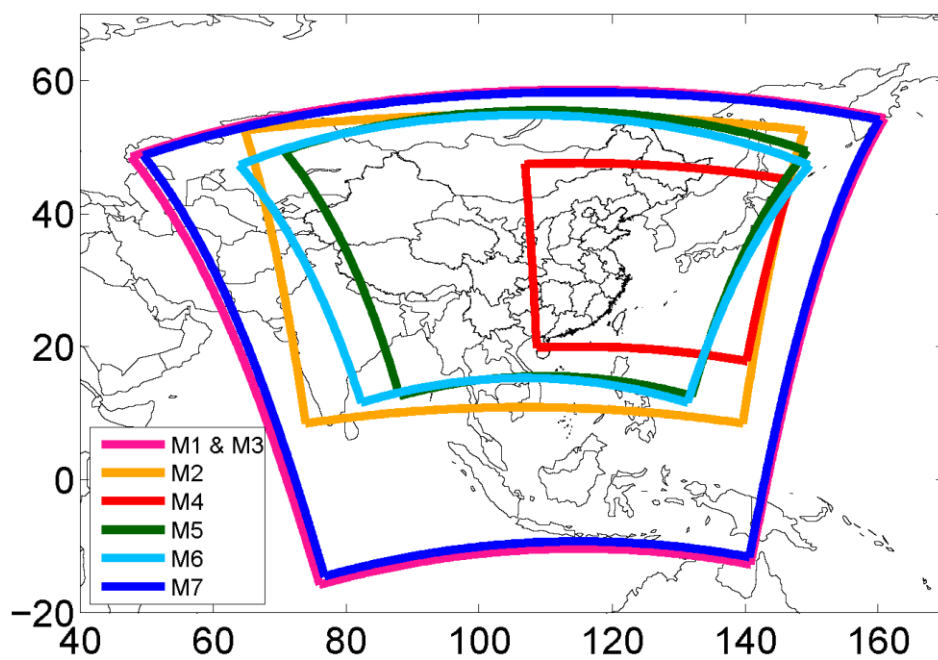


Figure 1. MICS-ASIA III Topic 3 modeling domains (descriptions of each model are documented in Table 1) M1: WRF-Chem 45km; M2: WRF-Chem 50km; M3: NU WRF 45km; M4: NU-WRF 15km; M5: RIEMS-IAP 60km; M6: RegCCMS 50km; M7: WRF-CMAQ 45km

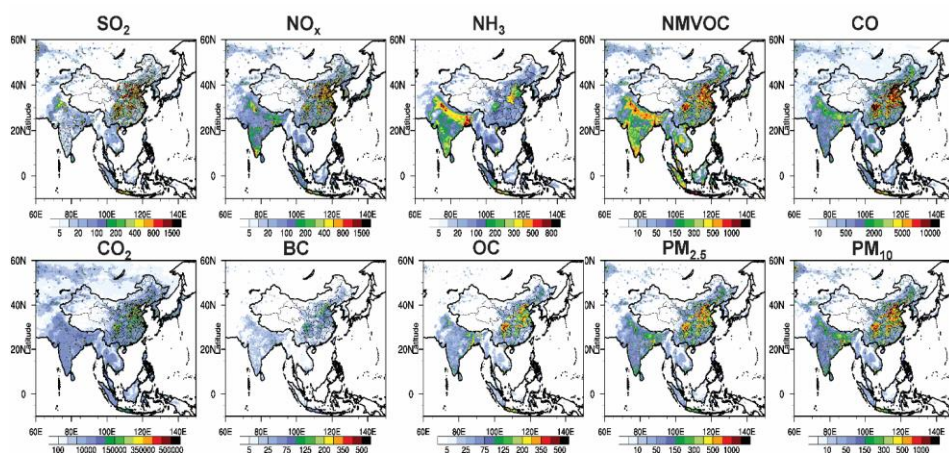


Figure 2. MIX emission inventory for January 2010 (Mg/month/grid)

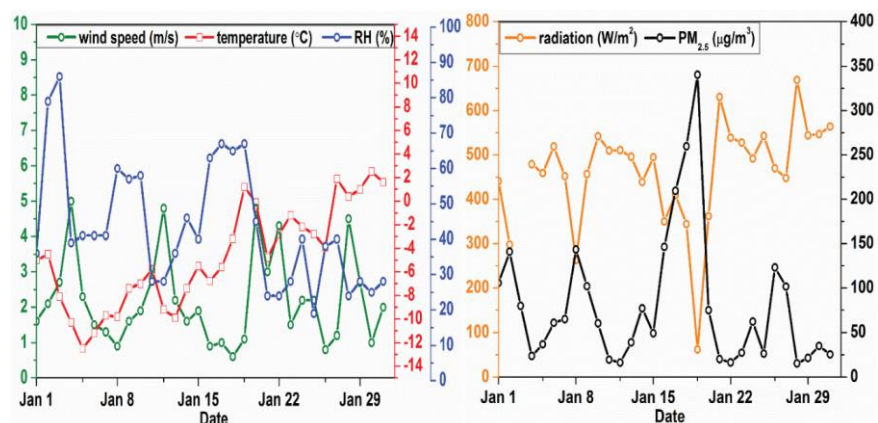


Figure 3. Observed near surface daily meteorological variables and $PM_{2.5}$ concentrations in Beijing for January 2010

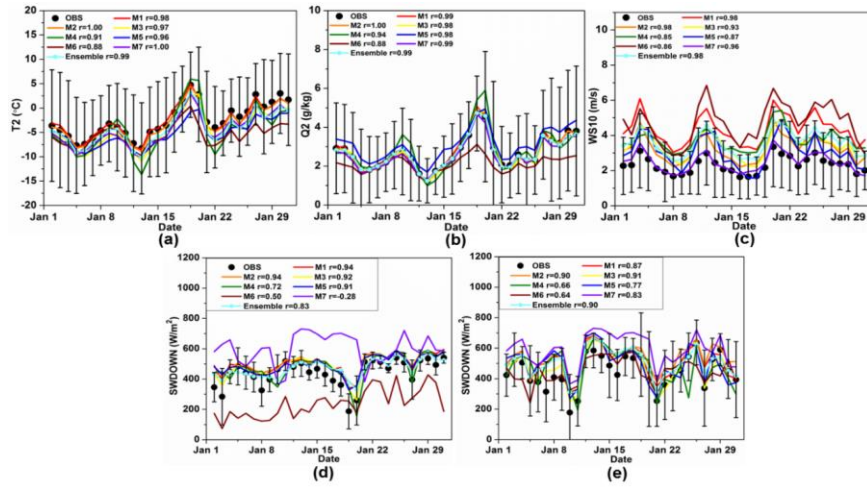


Figure 4. Comparisons between simulated and observed near surface temperature (a), water vapor mixing ratio (b), and wind speeds (c) (T2, Q2, and WS10), downward shortwave radiation in North China (d) and South China (e) (spatial daily values are averaged over measurements shown in S4 and S5; the error bars show the standard deviation of values over the measurement sites)

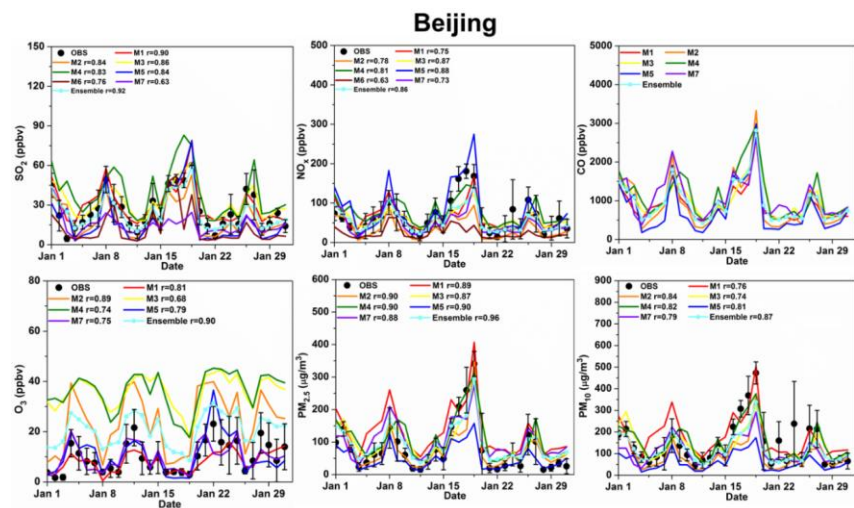


Figure 5. Comparisons between simulated and observed daily air pollutants (SO_2 , NO_x , CO , O_3 , $\text{PM}_{2.5}$ and PM_{10}) at the Beijing CARE-China site

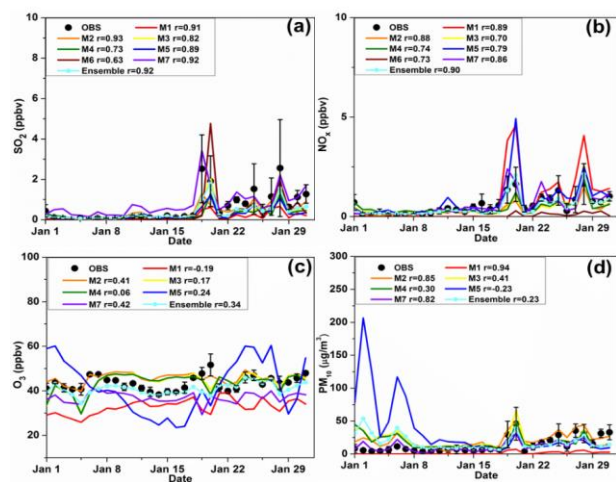


Figure 6. Comparisons between simulated and observed daily air pollutants (SO_2 , NO_x , O_3 , and PM_{10}) at the Rishiri EANET sites

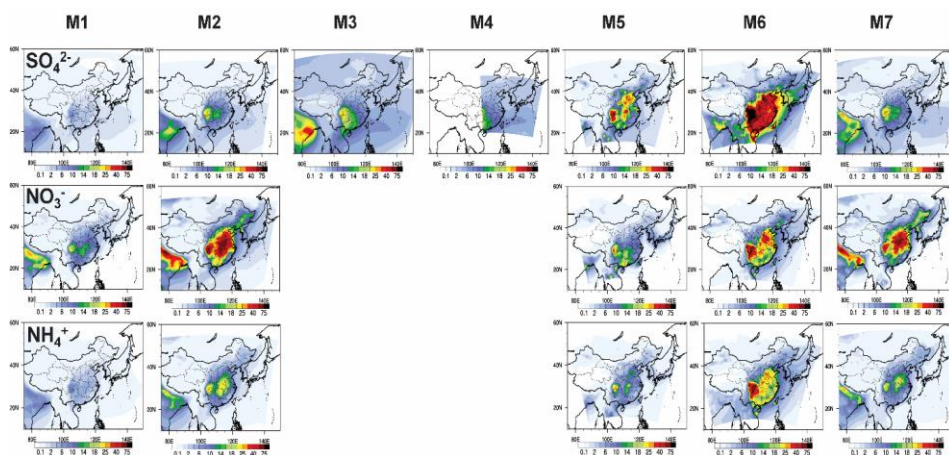


Figure 7. Simulated monthly concentrations of major PM_{2.5} components (μg/m³) for January 2010 from all participating models

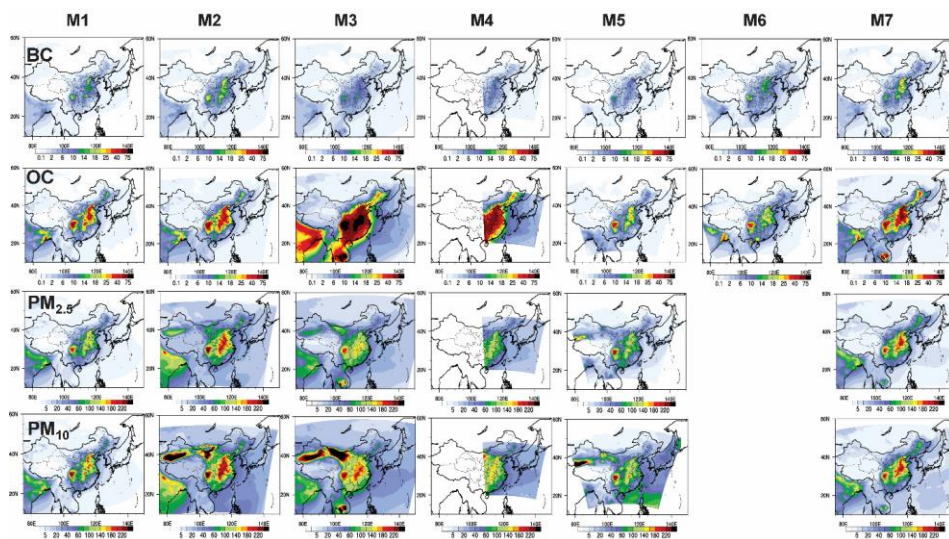


Figure 8. Simulated monthly concentrations of PM_{2.5} and major PM_{2.5} components (μg/m³) for January 2010 from all participating models

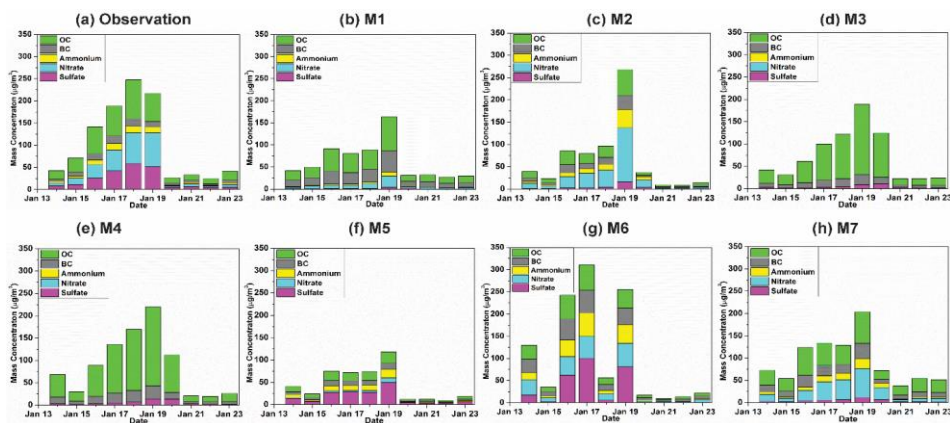


Figure 9. Observed and simulated daily mean concentrations of major PM_{2.5} chemical components in the urban Beijing site

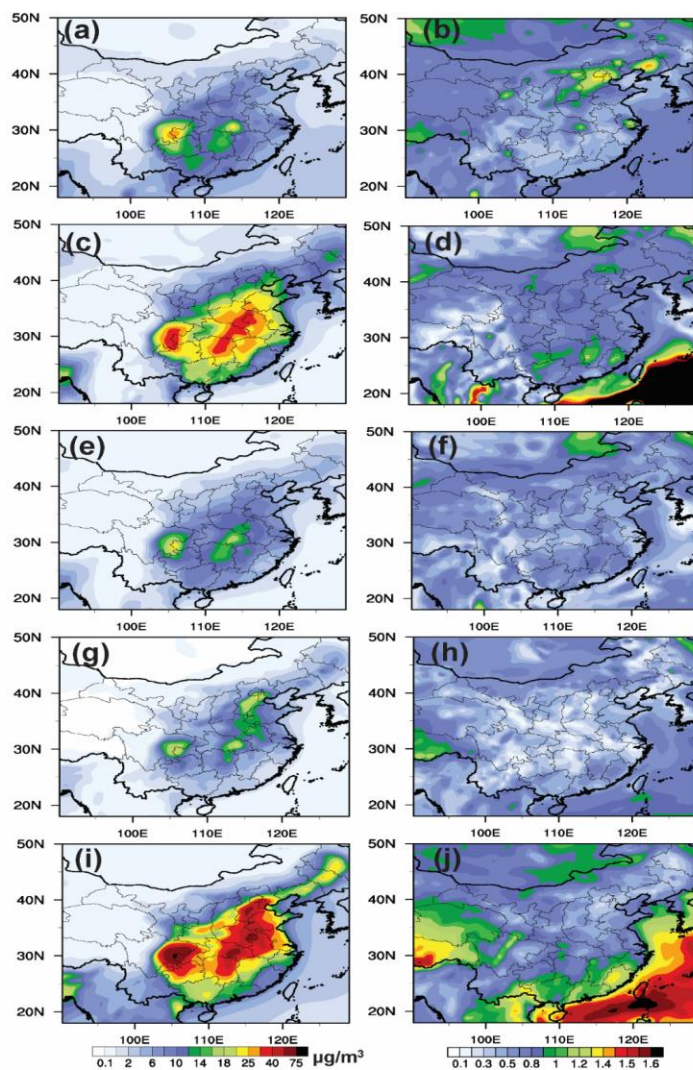


Figure 10. The ensemble mean monthly averaged near-surface distributions of $PM_{2.5}$ compositions for January 2010 (sulfate (a), nitrate (c), ammonium (e), BC (g), and OC (i)), along with the spatial distribution of the coefficient of variation ((b), (d), (f), (h), and (j), standard deviation divided by the average)

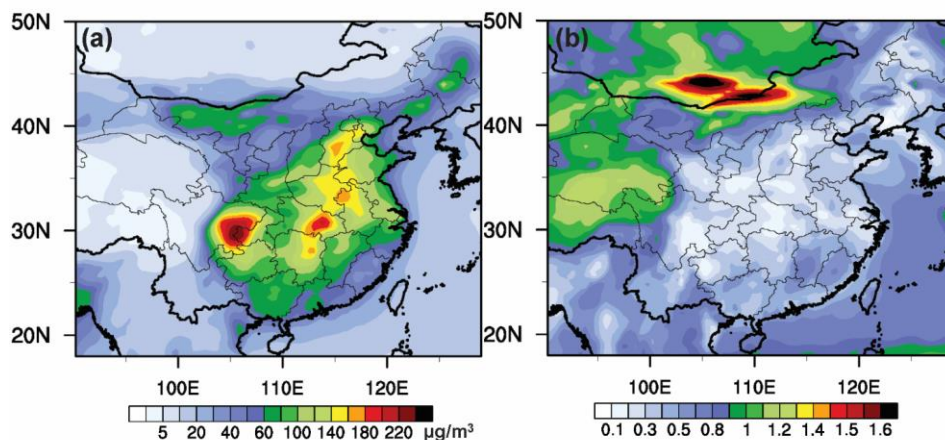


Figure 11. The ensemble mean monthly averaged near-surface distributions of $PM_{2.5}$ for January 2010 (a), along with the spatial distribution of the coefficient of variation (b, standard deviation divided by the average)

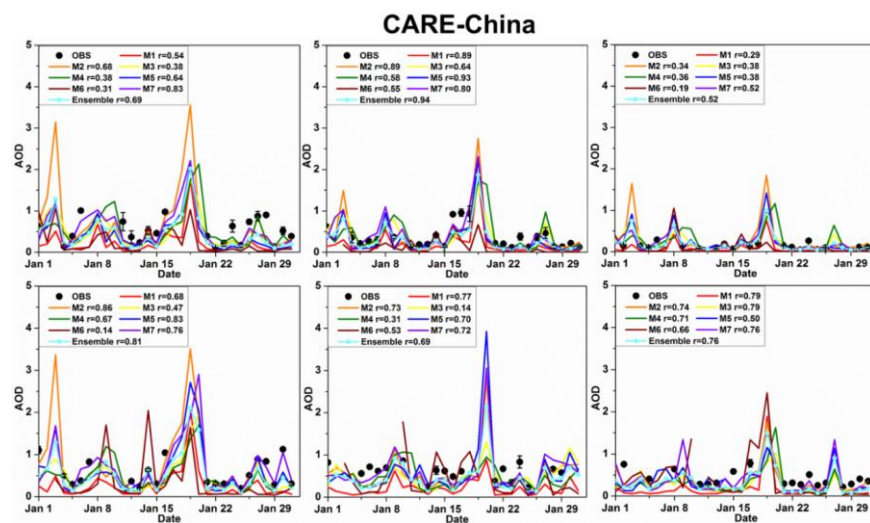


Figure 12. Comparisons between simulated and observed daily (daytime) mean AOD at the CARE-China sites (Baoding, Beijing City, Beijing Forest, Cangzhou, Jiaozhou, Shenyang,)

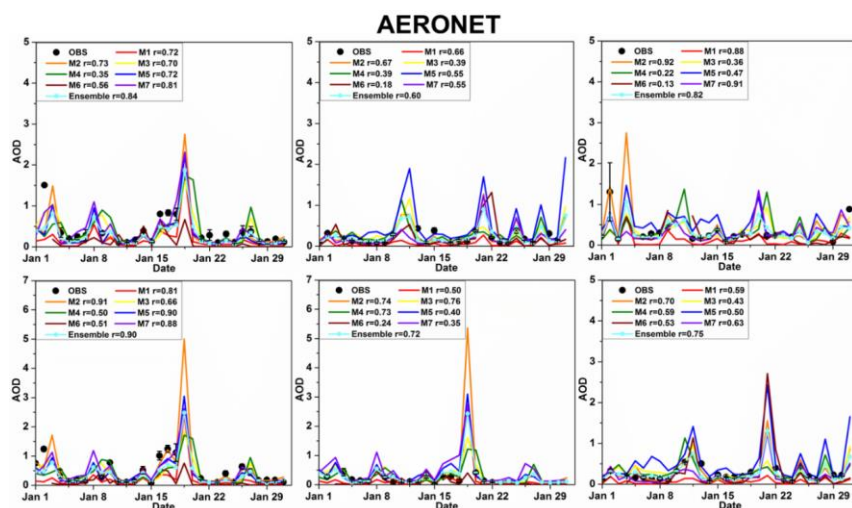


Figure 13. Comparisons between simulated and observed daily (daytime) mean AOD at the AERONET sites (Beijing, Shirahama, GIST, Xianghe, Xinglong, Osaka)